# Clathrin-mediated Endocytosis Facilitates Internalization of *Magnaporthe oryzae* Effectors into Rice Cells

Ely Oliveira-Garcia[1,2]*, Tej Man Tamang[1,3], Jungeun Park[3], Melinda Dalby[1], Magdalena Martin-Urdiroz[4], Clara Rodriguez Herrero[4,5], An Hong Vu[2], Sunghun Park[3], Nicholas J. Talbot[5] & Barbara Valent[1]*

[1]Department of Plant Pathology, Kansas State University, Manhattan, KS 66506, U.S.A.
[2]Department of Plant Pathology and Crop Physiology, Louisiana State University, Baton Rouge, LA 70803, U.S.A.
[3]Department of Horticulture and Natural Resources, Kansas State University, Manhattan, KS 66506, U.S.A.
[4]School of Biosciences, University of Exeter, Exeter, EX4 4QD, UK
[5]The Sainsbury Laboratory, Norwich Research Park, Norwich NR4 7UH, UK.

*Corresponding authors: E. Oliveira-Garcia; E-mail: EOliveiraGarcia@agcenter.lsu.edu and B. Valent; E-mail: bvalent@ksu.edu

## ABSTRACT

Many filamentous eukaryotic plant pathogens, such as fungi and oomycetes, deliver effectors into living plant cells to suppress defenses and control plant processes needed for infection. To date, little is known about the mechanism by which these pathogens translocate effector proteins across the plasma membrane into the plant cytoplasm. The blast fungus *Magnaporthe oryzae* secretes cytoplasmic effectors into a specialized biotrophic interfacial complex (BIC) before translocation. Here we show that cytoplasmic effectors within BICs are packaged into dynamic vesicles that can occasionally be found separated from BICs in the host cytoplasm. Live cell imaging with

fluorescently-labelled rice lines, showed that BICs are enriched in plant plasma membrane, actin, and Clathrin Light Chain-1, a marker for clathrin-mediated endocytosis (CME). We report that a novel cytoplasmic effector, Bas83, labels empty membrane vesicles surrounding BICs. Inhibition of CME using VIGS and chemical treatments results in a distinctive swollen BIC phenotype lacking effector vesicles. In contrast, fluorescent marker co-localization, VIGS and chemical inhibitor studies failed to implicate clathrin-independent endocytosis in effector vesicle formation. Taken together, this study provides evidence that cytoplasmic effector translocation is mediated by clathrin-mediated endocytosis in BICs and suggests a role for *M. oryzae* effectors in co-opting plant endocytosis.

## INTRODUCTION

Many fungal and oomycete pathogens cause plant disease by hijacking and feeding on living plant cells, and they deliver effectors into and around host cells to promote infection (Giraldo and Valent, 2013; Lo Presti and Kahmann, 2017). This includes the Ascomycete fungus *Magnaporthe oryzae* (synonym of *Pyricularia oryzae*), which threatens global food security by causing blast diseases on rice, on several millets, and most recently on wheat (Gladieux et al., 2018; Valent et al., 2020). *M. oryzae* executes a hemibiotrophic lifestyle involving biotrophic invasion of successive plant cells by specialized intracellular invasive hyphae (IH) that grow from cell to cell (Kankanala et al., 2007). Blast IH growing in living host cells are enclosed by extensions of the plant plasma membrane termed the extra-invasive hyphal membrane (EIHM). Colonized cells die as they fill with hyphae and the EIHM and host vacuolar membranes become disrupted, while the fungus moves on to colonize neighboring cells using the same strategy (Kankanala et al., 2007; Mochizuki et al., 2015; Sakulkoo et al., 2018; Jones et al., 2021). Each successful IH undergoes hyphal morphogenesis and is associated with differentiated interfacial zones after entering the host cell lumen (Kankanala et al., 2007; Khang et al., 2010). Specifically, appressorial penetration pegs enlarge into tubular filamentous hyphae, called primary invasive hyphae, which are enclosed in EIHM with an extended dome-shaped cap, the Biotrophic Interfacial Complex (BIC). BICs accumulate cytoplasmic effectors destined for translocation into the host cytoplasm. Primary hyphae then transition to a bulbous pseudohyphal-like growth form. BICs at the tips of primary hyphae are left behind beside the first bulbous IH cell during the differentiation process but they continue to accumulate cytoplasmic effectors as the bulbous IH grow to fill the cell (Khang et al.,

64 2010). Mutation in an effector gene, Required-for-Focal-BIC-Formation 1 (*RBF1*), encoding a
65 glycine-rich secreted protein, results in dispersed cytoplasmic effector localization around BIC-
66 associated cells (the primary hyphae and first bulbous IH cell), perturbs primary hyphal structure,
67 and decreases pathogenicity (Nishimura et al., 2016; Nishizawa et al., 2016).

68 In blast disease, cytoplasmic and apoplastic effectors are clearly differentiated by the
69 fungal secretion system used and their localization pattern after secretion. Primary hyphae and the
70 first bulbous IH focally secrete cytoplasmic effectors into BICs using a specialized, Golgi-
71 independent secretion system that is insensitive to treatment with Brefeldin A (BFA), a chemical
72 that inhibits conventional Golgi-mediated secretion in fungi (Giraldo et al., 2013; Van den
73 Ackerveken, 2017; Wang et al., 2017). Fluorescent cytoplasmic effectors are routinely detected in
74 the cytoplasm of invaded cells, and some are also detected in the cytoplasm of surrounding
75 uninvaded host cells, apparently moving through plasmodesmata to prepare surrounding cells
76 before invasion (Khang et al., 2010). In contrast, apoplastic effectors, such as the biotrophy-
77 associated secreted protein 4 (Bas4), the LysM protein 1 (Slp1), and Bas113, are secreted via
78 conventional golgi-mediated secretion, and they accumulate uniformly throughout the apoplastic
79 compartment enclosed within the EIHM, outlining the entire IH without bleeding into the plant
80 cell wall (Mosquera et al., 2009; Mentlak et al., 2012; Giraldo et al., 2013). Indeed, localization of
81 secreted Bas4 fluorescent fusion proteins has become a reliable live cell imaging marker for the
82 intactness of the EIHM around IH (Khang et al., 2010; Mochizuki et al., 2015; Jones et al., 2021).
83 After filling the host cell, hyphal differentiation and BIC relocalization recur for each new hypha
84 that enters a living neighbor cell (Khang et al., 2010; Sakulkoo et al., 2018).

85 The mechanism by which eukaryotic filamentous plant pathogens deliver effectors across
86 the host plasma membrane inside living host cells is poorly understood and the mechanism is likely
87 to vary in different systems (Giraldo and Valent, 2013; Petre and Kamoun, 2014; Fawke et al.,
88 2015; Lo Presti et al., 2015; Lo Presti and Kahmann, 2017). Amino acid translocation motifs have
89 been identified for oomycete effectors, with the RXLR motif being the most common, although
90 cell entry motifs for fungal effectors have not been defined. The RXLR motif in oomycete effectors
91 was reported to mediate host cell uptake through endocytosis based on binding to
92 phosphatidylinositol-3-phosphate (PI3P) in host membrane (Kale et al., 2010), although it was
93 recently shown that the RXLR motif from *Phytophthora infestans* effector AVR3a is cleaved off
94 before secretion from the pathogen (Wawra et al., 2017). Therefore, the function of RXLR motif

95 in cell entry remains disputed (Petre and Kamoun, 2014; Trusch et al., 2018). Another amino acid
96 motif, YKARK, appears involved in translocation of the effector SpHtp3 from *Saprolegnia*
97 *parasitica*, a serious oomycete pathogen of fish, inside fish cells (Trusch et al., 2018). Specifically,
98 this effector appears to be internalized inside host cells via lipid-raft mediated endocytosis through
99 binding to a gp96-like receptor, and another effector is involved in releasing SpHtp3 from vesicles
100 into the fish cytoplasm. In an example from a fungal pathogen, a solvent-exposed RGD
101 vitronectin-like motif is required for internalization of ToxA, a host-specific proteinaceous toxin
102 secreted by the necrotrophic wheat pathogen *Pyrenophora tritici-repentis* (Manning and Ciuffetti,
103 2005). In addition to uptake by plant endocytosis, effectors might enter plant cells through
104 specialized translocon complexes in the plasma membrane. For example, the human malaria
105 parasite, *Plasmodium falciparum*, is contained within a parasitophorous vacuole inside invaded
106 red blood cells, and effectors are delivered across the membrane into the host cytoplasm by the
107 PTEX translocon (Elsworth et al., 2014). Recently, a stable protein complex comprised of five
108 unrelated fungal effectors and two fungal membrane proteins has been implicated in effector
109 translocation by the maize smut fungus *Ustilago maydis* (Ludwig et al., 2021). However, the
110 question of how effectors are taken up into plant cells remains largely unresolved for eukaryotic
111 plant pathogens.

112 Clathrin-mediated endocytosis (CME) is the major mechanism by which eukaryotic cells
113 internalize extracellular or membrane-bound cargoes, and this process is best understood in
114 mammalian systems and yeast (Kaksonen and Roux, 2018). Increasing understanding of CME in
115 plants shows both conserved and evolutionarily unique mechanistic details (Qi et al., 2018;
116 Reynolds et al., 2018; Johnson et al., 2020; Narasimhan et al., 2020). CME is known to play key
117 roles in plant-microbe interactions (Dodds and Rathjen, 2010; Beck et al., 2012; Fan et al., 2015).
118 CME is required for immunity mediated by pattern recognition receptor kinases, for instance,
119 specifically through internalization of activated extracellular pattern recognition receptors (PRRs)
120 for degradation in the vacuole (Mbengue et al., 2016). Examples include the pattern recognition
121 receptor Pep receptor 1/2 (PEPR1/2), the EF-TU receptor (EFR) recognizing the PAMP bacterial
122 elongation factor, and FLS2 recognizing the PAMP flagellin (flg-22) (Spallek et al., 2013;
123 Mbengue et al., 2016), as well as the Cf-4 receptor-like protein that recognizes the *C. fulvum* Avr4
124 avirulence effector (Postma et al., 2016). Trafficking of activated PRRs requires clathrin and
125 converges onto endosomal vesicles that are also shared by the hormone receptor Brassinosteriod

126 Insensitive 1 (BRI1). Additionally, it is known that pathogens can control plant CME. In addition
127 to its role in suppressing INF1-mediated cell death, the *P. infestans* host-translocated RXLR
128 effector AVR3a was recently shown to associate with the Dynamin-Related Protein 2, a plant
129 GTPase implicated in receptor-mediated endocytosis, and to suppress flg22-triggered defense
130 responses and reduce FLS2 internalization (Chaparro-Garcia et al., 2015). Therefore, AVR3a
131 interacts with a membrane-remodeling complex involved in immune receptor-mediated
132 endocytosis. Also, in host cells containing haustoria from the oomycete *P. infestans*, the late
133 endosomal pathway is rerouted from the vacuole to the extrahaustorial membrane (EHM)
134 surrounding haustoria (Bozkurt et al., 2015). Multiple effectors from this pathogen are now
135 implicated in rerouting the host membrane trafficking system and autophagy machinery for the
136 benefit of the invading pathogen (Bozkurt et al., 2015; Dagdas et al., 2018; Petre et al., 2021).
137 Effector translocation in the *M. oryzae*/rice pathosystem is easily assayed by live cell
138 imaging of fluorescently-labeled effector proteins inside host cells after secretion by IH invading
139 rice leaf sheath cells (Khang et al., 2010). Although some effectors naturally localize to host nuclei,
140 addition of a nuclear localization signal (NLS) to fluorescent effectors enhances visualization of
141 translocation and cell-to-cell movement. Blast cytoplasmic effectors apparently do not contain a
142 translocation motif as reported for oomycete effectors. Instead, preferential accumulation in the
143 BIC, which is a prominent feature of the blast fungus-rice cell interface, is the major predictor of
144 translocation into the rice cell. Previously, the Nishizawa lab reported that a cytoplasmic effector
145 is packaged in vesicles in the outer region of the BIC (Mochizuki et al., 2015; Nishimura et al.,
146 2016; Nishizawa et al., 2016). Here, we have used live-cell fluorescence imaging to characterize
147 the nature and dynamics of membrane-bound effector vesicles within BICs and in surrounding
148 host cytoplasm. We show that BICs are enriched for CME components, and we report functional
149 analyses using virus-induced gene silencing (VIGS) and pharmacological approaches. When
150 considered together, our data indicate that blast effectors are internalized through clathrin-
151 mediated endocytosis in the outer BIC layers, followed by escape from the vesicles into the rice
152 cytoplasm.
153
154 **RESULTS**
155
156 **BICs contain multiple vesicles labeled by cytoplasmic effectors**

157 BICs were previously reported as interfacial structures containing fluorescently-labelled
158 apoplastic effectors, such as Bas4:eGFP, in an inner base layer and a concentration of fluorescent
159 cytoplasmic effectors in the outer 'dome-shaped' region (Khang et al., 2010; Nishizawa et al.,
160 2016). We now routinely resolve the dome region of BICs by laser confocal imaging as a
161 concentration of vesicles containing fluorescent cytoplasmic effectors (Figure 1). These effector
162 vesicles are illustrated by an image of a BIC at the tip of a primary hypha (tip-BIC) expressing
163 fluorescent apoplastic effector Bas4:eGFP and fluorescent cytoplasmic effector Pwl2:mRFP
164 (Figure 1A). The Bas4:eGFP fluorescence remains evenly distributed throughout the EIHM matrix
165 around the growing IH, including in the inner layer of the BIC. In contrast, Pwl2:mRFP occurs as
166 distinct vesicles in the outer BIC region. We have observed effector vesicles in tip-BICs labeled
167 with additional translocated effectors Bas1 and Pwl1 fused to either eGFP or mRFP (Supplemental
168 Figure S1). Vesicles are also observed after tip-BICs move beside the first bulbous IH cells (side-
169 BICs) (Figure 1B). We evaluated the proximity of these vesicles relative to both tip- and side-
170 BICs. Whereas the vast majority of vesicles associated with primary IH were located in the tip-
171 BIC, some vesicles associated with side-BICs were found in regions of the cytoplasm at least 7
172 µm from the fungal cell wall at the BIC, which we define as outside the BIC (Figure 1C). Inclusion
173 of the apoplastic effector Bas4:eGFP in these experiments confirmed that the EIHM remained
174 intact at each infection site, based on its outlining of the IH and lack of spilling into the invaded
175 rice cell.

176 We identified a novel cytoplasmic effector, Bas170 (MGG_07348.6), that localized in
177 vesicles in the rice cytoplasm short distances from the appressorial penetration site at a stage before
178 primary hyphal growth is visible. The Bas170:mRFP fusion protein naturally accumulates in the
179 rice nucleus at this early infection stage, presumably to reprogram plant transcription essential for
180 *M. oryzae* infection (Supplemental Figure S2). These results suggest rapid effector translocation
181 from appressoria even before growth of primary IH. Bas170:mRFP also labels BIC-associated
182 vesicles in tip-BICs, and vesicles have been observed at a distance from the BIC in later stages.
183 Vesicles observed using fluorescent Bas170 fusion proteins are similar to vesicles observed with
184 Pwl2, Pwl1 and Bas1 fusion proteins except that these latter effectors were not observed under
185 appressoria at the earlier time period.

186 **Vesicles in BICs are dynamic through time**

187 To understand vesicle dynamics in BICs through time, we imaged BIC effector fluorescence
188 during the morphogenic switch from tubular primary hyphae to bulbous IH, using a strain co-
189 expressing two cytoplasmic effectors, Bas1:eYFP and Pwl2:mRFP (Figure 2). The vesicle content
190 varied over the 2-hour period when the BIC was displaced from the primary hyphal tip to beside
191 the differentiating bulbous IH cell. Tip-BICs often contained vesicles with either red or green
192 fluorescence, rather than yellow, suggesting that effectors can be sorted into different vesicles. For
193 this series of experiments, Pwl2:mRFP occurred in vesicles that reached outer layers of the tip-
194 BIC compared to Bas1:eYFP. Pwl2:mRFP appeared less abundant relative to Bas1:eYFP during
195 the switch from tip- to side-BIC, recovering again after growth of bulbous IH (Figure 2A). Both
196 vesicle size and content varies within BICs through time (Figure 2 B-C). Specifically, BICs at
197 primary hyphal tips contain a larger number of smaller vesicles (Figure 2D,E). Whereas BICs on
198 primary hyphae deliver effectors in 'micro-vesicles' ranging from 41 nm to 114 nm, BICs on
199 mature bulbous hypha contain effectors in 'macro-vesicles' ranging from 153 nm up to 2310 nm
200 at times (Figure 2C,D). Effector vesicles beside mature bulbous IH often showed colocalization of
201 fluorescence from different effectors compared to vesicles in tip-BICs (Figure 2A, B and F).
202 Cytoplasmic connections were observed between BICs and plant cytoplasm at the
203 periphery of the invaded cell, illustrated in optical sections through a BIC in Supplemental Movie
204 S1. This is consistent with a previous report of dynamic connections linking BICs and host
205 cytoplasm underneath the appressorium (Khang et al., 2010). These cytoplasmic connections may
206 facilitate delivery of effectors from cytoplasm surrounding the BIC in the cell center to the
207 peripheral cytoplasm, in position to rapidly move through plasmodesmata into neighboring cells.

208 **BIC vesicles contain plant plasma membrane**

209 Effector-labeled vesicles in the BIC could arise through secretion of cytoplasmic effectors in
210 exosomes by the fungus or through plant endocytosis. We previously reported that BICs contain
211 material derived from plant plasma membrane based on infection of transgenic rice expressing a
212 plasma membrane marker (Giraldo et al., 2013). Here we again use LTi6B:GFP-labeled rice to
213 confirm that BICs contain abundant plant plasma membrane (Figure 3A,B). Individual effector
214 vesicles were observed to be surrounded by labeled plant plasma membrane (Fig 3C), especially
215 for vesicles in side-BICs on mature bulbous hyphae, where the vesicles reach diameters of 150 nm
216 or larger.

217 To confirm that BIC vesicles contain plant plasma membrane, we evaluated the BIC
218 membrane composition by staining with the endocytosis tracker dyes FM 4-64 and FM 1-4 (Fig 3
219 D,E). These amphiphilic styryl dyes insert in the plasma membrane where they diffuse laterally in
220 the membrane and are only internalized into the cell via endocytosis (Atkinson et al., 2002; Bolte
221 et al., 2004). We previously showed that FM 4-64 is prevented from inserting in IH membranes,
222 which are sealed inside the EIHM (Kankanala et al., 2007). Rice treated with FM 4-64 and FM 1-
223 43 undergoing infection by *M. oryzae* strain KV177 or KV209 showed massive accumulation of
224 both dyes in BICs. Exclusion of these dyes from the hyphal membranes was documented by the
225 lack of fluorescent labeling of the fungal septa and vacuoles, which occurs if the dye inserts in the
226 fungal plasma membrane (Atkinson et al., 2002; Kankanala et al., 2007). Images of BICs stained
227 with FM 4-64 showed vesicles carrying effectors immersed in the region of intense FM 4-64
228 staining associated with the BIC (Figure 3E). Vesicles that carry effectors were also observed
229 separated from the BIC, presumably in the rice cytoplasm (Figure 3E, inset upper right), but
230 effector-containing vesicles have not been frequently observed at long distances from the BIC
231 (Supplemental Movie S2). Apparent vesicular bursting was also observed, which suggests that the
232 vesicles are unstable, presumably releasing the effector contents into the host cytoplasm. Taken
233 together, these results indicate that BIC-associated effector vesicles are more likely derived
234 through plant endocytosis than from secretion of fungal exosomes.

235 **Bas83 is a unique cytoplasmic effector that associates with rice membrane concentrating**
236 **around BICs**

237 Since it is likely that specific blast effectors play roles in vesicle formation and effector
238 translocation, we were particularly interested in effectors that appear to associate with membranes
239 in host cells. The *BAS83* (MGG_08506.6) gene is unique to *M. oryzae*, and it is 36-fold upregulated
240 during biotrophic invasion (Mosquera et al., 2009). Bas83 is a cytoplasmic effector that is secreted
241 by the fungus using the Golgi-independent secretion pathway identified for other cytoplasmic
242 effectors (Giraldo et al., 2013). Bas83:mRFP is translocated into invaded host cells, but it does not
243 precisely colocalize with other BIC-localized cytoplasmic effectors Pwl2:eGFP and Pwl1:eGFP
244 (Figure 4A; Supplemental Figure S3), and it does not move ahead into uninvaded neighboring
245 cells as these other effectors do. In contrast, Bas83:mRFP seems to label the EIHM surrounding
246 the BIC-associated cells, the primary hyphae and first bulbous IH, and it labels membrane bubbles,
247 or vesicles, near to BICs and BIC-associated cells (Figure 4A-C). Figure 4A shows that

248 Bas83:mRFP-labeled vesicles do not contain the cytoplasmic effector Pwl2:eGFP, indicating they
249 are distinct from effector vesicles in BICs. Bas83:mRFP is also associated with vesicles observed
250 under appressoria (Figure 4C; Supplemental Figure S3). However, Bas83:mRFP fails to label
251 membrane surrounding subsequently formed bulbous IH that are associated with apoplastic
252 effectors and not with cytoplasmic effectors (see 2nd bulbous IH in Figure 4C). We hypothesize
253 that Bas83 is involved in recruiting new plant plasma membrane to form the EIHM and BICs
254 during biotrophic development. However, repeated attempts in two different laboratories (264
255 purified transformants, 4 methods and 5 experiments; KSU and Univ. of Exeter) failed to produce
256 knock-out mutants for further functional analysis.

257 **BICs contain plant actin**

258 The actin cytoskeleton is essential for endocytic processes including plasma membrane folding,
259 vesiculation, and vesicle transport (Grassart et al., 2014; Narasimhan et al., 2020). Effector vesicle
260 formation in BICs suggests that this interfacial structure should contain abundant host actin.
261 Therefore, we imaged plant actin dynamics during biotrophic invasion using rice lines expressing
262 the actin marker LifeAct:eGFP. Infection by *M. oryzae* strains expressing chimeric protein
263 Pwl2:mRFP showed massive colocalization of LifeAct:eGFP in BICs (Figure 5A). Actin was
264 abundant in all imaged tip- and side-BICs (Figure 5B). Likewise, colocalization of fluorescent
265 Phalloidin conjugates and fluorescently-labeled effector confirmed that BICs are rich in plant actin
266 filaments (Figure 5C). We hypothesize that actin filaments are responsible for plasma membrane
267 manipulation, vesiculation and possibly for the transport of those vesicles carrying effectors into
268 the rice cell cytoplasm.

269 **BICs contain abundant plant clathrin, but not flotillin**

270 Clathrin-mediated endocytosis (CME) is the major endocytosis mechanism in plants, with some
271 contribution by Clathrin-independent endocytosis (CIE) (Chen et al., 2011; Ewers and Helenius,
272 2011; Fan et al., 2015; Narasimhan et al., 2020). To assess co-localization of specific endocytosis
273 markers with BICs, we generated transgenic rice lines expressing a fluorescent marker for either
274 CME or CIE. For CME, we generated a C-terminal translational fusion of eGFP with the rice
275 Clathrin light chain-1 (OsCLC1), which is a component of the clathrin coat together with clathrin
276 heavy chain. Rice lines expressing OsCLC1:eGFP show typical clathrin foci (Konopka et al.,
277 2008; Narasimhan et al., 2020) in uninfected rice cells (Figure 6A). The marker for CIE was a C-

278 terminal translational fusion of eGFP to flotillin (Flot1), which is a component of lipid rafts (Otto
279 and Nichols, 2011; Li et al., 2012). Rice lines with the CME and CIE markers were used for leaf
280 sheath assays with an *M. oryzae* strain expressing Pwl2:mRFP to label BICs. In addition to typical
281 clathrin foci around the cell periphery, all tip-BICs and side-BICs contain fluorescence from
282 OsCLC1:eGFP co-localizing with Pwl2:mRFP (Figure 6 A,B). Clathrin fluorescence could
283 sometimes be observed co-localizing with effector fluorescence in BIC vesicles (Supplemental
284 Movie S3). In contrast, no tip-BICs colocalized with Flot1:eGFP. Some colocalization of
285 Flot1:eGFP and Pwl2:mRFP occurred in side-BICs besides mature bulbous hyphae (Figure 6B).
286 Colocalization results from several independent experiments were consistent with a major role for
287 CME, but not for CIE, in the internalization of cytoplasmic effectors.

288 **Silencing of rice endocytosis machinery blocks *M. oryzae* infection**

289 We assessed the impact of inhibition of CME and CIE on BICs and effector vesicles using the
290 brome mosaic virus system (Ding et al., 2006; Ding et al., 2007) for silencing of genes for CME
291 and CIE components that have been characterized by gene silencing analyses in *Arabidopsis*.
292 Specifically, we silenced two rice CME genes, Adaptor protein complex-2 subunit α2 (*AP-2α*) and
293 clathrin heavy chain-1 (*CHC1*) (Di Rubbo et al., 2013; Larsson et al., 2017) as well as the CIE
294 gene *Flotillin-1* (*Flot1*) (Li et al., 2012). Silencing of both *AP-2α* and *CHC1* resulted in severe
295 reduction in pathogenicity in whole plant spray inoculation assays (Figure 7 A,B). However, as
296 expected, silencing of these genes caused stunting and decreased plant health (Supplemental
297 Figure S4), and levels of pathogenicity in blast disease are known to be decreased on unhealthy
298 rice plants. More significant is the phenotype of pathogen blockage at individual infection sites.
299 Inhibition of clathrin-mediated endocytosis led to a distinctive swollen BIC phenotype, with
300 enlarged, abnormally-shaped BICs that lack effector vesicles. By contrast, silencing of the CIE
301 marker gene *Flot1* showed minor effects on pathogenicity (Figure 7A,B), and had little impact on
302 BIC structure [Figure 7C,F; compare 26 hpi RNAi*Flot1* (CIE) and RNAi*AP-2α* (CME)].

303 In addition to swollen BICs as sites with primary hyphae, silencing of both CME genes
304 decreased appressorial penetration and induced the accumulation of the cytoplasmic effector
305 Pwl2:mRFP under failed penetration sites where it is not normally observed (Figure 7D,E). In
306 contrast, silencing of Flot1 had only minor effects on appressorium penetration success and on
307 accumulation of Pwl2:mRFP under failed appressoria. Like our finding of early accumulation of
308 Bas170 under appressoria before penetration, these results again suggest that effector uptake

309 begins before host penetration. These results also suggest that effector uptake at the appressorial
310 penetration stage and from BICs is mediated by CME.

311 **Chemical inhibition of rice endocytosis machinery blocks *M. oryzae* infection**

312 Pharmacological approaches have impacted studies in diverse biological systems (Robinson et al.,
313 2008; Hicks and Raikhel, 2010; Grassart et al., 2014; Fan et al., 2015). To further assess potential
314 impact of the plant endocytic machinery on cytoplasmic effector translocation, we tested a series
315 of chemicals that are reported to inhibit plant CME or CIE (Table 1). Compared with the non-
316 treated control (Figure 8A), treatment with reported CME inhibitor cantharidin led to abnormally-
317 shaped, swollen BICs resembling those seen with silencing of CME components (Figure 8B).
318 Fluorescence intensity linescans confirm that cantharidin treatment had no impact on localization
319 of apoplastic effector Bas4:eGFP in the base of the BIC.

320 Subsequent quantification of cantharidin treatment along with treatment of 2 additional
321 reported CME inhibitors, chlorpromazine and triclosan (Table 1), showed a high proportion of
322 swollen, irregular-shaped cytoplasmic effector fluorescence patterns in BICs (Figure 9A-C). By
323 contrast, inhibition of CIE with filipin and methyl-β-cyclodextrin resulted in minor to no effect on
324 BIC effector fluorescence patterns (Figure 9A-C). Two chemical inhibitors with potential CME
325 association (Table 1) show different impacts on BIC effector fluorescence patterns. Wortmannin,
326 which inhibits phosphatidylinositol 3-kinase (PI 3-kinase) and is implicated in late endosomal
327 trafficking (Robinson et al., 2008) had a major impact on BIC structure, while concanamycin A,
328 which inhibits vacuolar-type ATPase and induces vacuolar acidification (Robinson et al., 2008),
329 had little impact on BIC structure (Figure 9A-C).

330 Moreover, treatment with CME inhibitors cantharidin, chlorpromazine and triclosan, but
331 not with CIE inhibitors filipin and methyl-β-cyclodextrin, resulted in reduced appressorial
332 penetration and induced abnormal accumulation of the cytoplasmic effector Pwl2:mRFP under
333 appressorial penetration sites where it is not normally observed (Figure 9A - compare 18 hpi CIE
334 and CME inhibitors; Figure 9D,E). Wortmannin, but not concanamycin A, also impacted
335 appressorial function and resulted in abnormal Pwl2:mRFP accumulation under appressoria. These
336 results support our findings with Bas170:mRFP (Supplementary Figure 2) in suggesting that
337 effector uptake begins before or at the point that host penetration occurs. Indeed, chemical
338 inhibition of endocytosis in rice cells undergoing *M. oryzae* infection mimics the results obtained
339 with VIGS, further supporting a role for CME in effector uptake into rice cells.

340

341 **DISCUSSION**

342 Our results, when taken together, provide strong evidence that cytoplasmic effector translocation
343 is BIC-localized and mediated by CME. We report that diverse cytoplasmic effectors occur in
344 dynamic vesicles in tip-BICs associated with primary hyphae that first colonize host cells and then
345 in BICs that remain beside the first bulbous IH after hyphal differentiation. Tip-BICs contain many
346 small effector micro-vesicles (~87 nm) and co-expression of differentially-labeled effectors
347 Bas1:eYFP and Pwl2:mRFP showed these effectors can be sorted into different vesicles (Figure
348 2). Vesicle composition can be seen to vary as tip-BICs move to become side-BICs during hyphal
349 differentiation. Specifically, side-BICs contained fewer, larger vesicles that reach >500 nm in
350 diameter and show co-localization of Bas1:eYFP and Pwl2:mRFP. Our results confirm a previous
351 report that cytoplasmic effectors occur in ~500 nm vesicles in the outer BIC domes beside bulbous
352 IH (Mochizuki et al., 2015; Nishimura et al., 2016; Nishizawa et al., 2016). We also observed
353 effector vesicles in the host cytoplasm at short distances from maturing side-BICs (Figure 2).
354 Release of effectors from these vesicles into the host cytoplasm would require a special
355 mechanism, perhaps mediation by an effector as suggested for release of the *S. parasitica* effector
356 from endocytic vesicles into the fish cell cytoplasm (Trusch et al., 2018).

357 We report that BICs producing effector vesicles contain multiple hallmarks of active
358 clathrin-mediated endocytosis (CEM), including focal accumulation of fluorescently-labelled
359 Clathrin Light Chain-1 (CLC1), a key subunit of the clathrin coat in CME (Figure 6). Focal
360 accumulation of actin in the BICs, as detected in stable transgenic plants expressing LifeAct:eGFP
361 and by staining with rhodamine-labeled phalloidin (Figure 5), is consistent with a role in CME,
362 although it was recently reported that actin plays a different role in CME in plants than in the well-
363 studied systems in mammals and yeast (Qi et al., 2018; Johnson et al., 2020; Narasimhan et al.,
364 2020). We confirm that BICs contain abundant rice plasma membrane (Giraldo et al., 2013) using
365 transgenic plants expressing fluorescent plasma membrane fusion protein LTi6b:eGFP, and using
366 the amphiphilic stryryl dyes FM 4-64 or FM 1-43 to track membranes that are internalized by
367 endocytosis (Bolte et al., 2004). Indeed, we obtained occasional views of effector vesicles ringed
368 in LTi6b:eGFP or FM 4-64 labeled membrane (Figure 3C). Interestingly, we identified a novel
369 effector, Bas83, that labels non-effector vesicles and EIHM focused around BICs and the BIC-
370 associated cells, which could be involved in replenishing host membranes needed for extensive

371 endocytotic activity in the BIC (Figure 4; Supplemental Figure S3). In contrast, flotillin
372 (Flot1:eGFP), which is a component of lipid raft-mediated clathrin independent endocytosis, rarely
373 co-localizes with tip-BICs where active translocation is occurring (Figure 6C). Our fluorescent
374 marker co-localization experiments are all consistent with BICs as a focused area of CME.

375 For functional analyses of the role of endocytosis in effector translocation, we performed
376 transient silencing of two rice CME components, Clathrin Heavy Chain-1 (CHC-1) and Adaptor
377 Protein Complex subunit 2α (AP-2α), as well as silencing of the CIE component Flotillin-1. We
378 also used 7 pharmacological agents that are reported to inhibit or be associated with CME or CIE
379 endocytosis in plants. Both strategies have potential problems. Rice plants that received the CHC-
380 1 and APC-2 silencing vectors were significantly reduced in rice blast symptom, compared to the
381 empty vector control and to Flot1-silenced lines (Figure 7; Supplemental Figure S4). However,
382 this could be due, at least in part to inevitable health costs to the plant through silencing component
383 genes for essential cellular processes. Unhealthy rice plants are generally less susceptible to blast
384 disease (Kato, 1974). Additionally, care must be taken in the interpretation of results in
385 pharmacological studies based on new evidence that endocytosis inhibitors characterized in
386 mammalian systems may not have the same targets in plants (Dejonghe et al., 2016), and
387 pharmacological agents also have off-target effects (Hicks and Raikhel, 2010; Dejonghe and
388 Russinova, 2017). However, both studies complement each other in that transient silencing of the
389 two CME components and treatment with 4 different pharmacological agents associated with CME
390 gave the same swollen BIC phenotype, in which labeled fluorescent effectors accumulate in
391 abnormally-sized BICs lacking the discreet effector vesicles seen in control infection sites (Figure
392 8 and 9). In contrast, transient silencing of the CIE component Flotilin-1 and treatment with
393 pharmacological inhibitors associated with CIE show little or no impact on BIC vesicular structure
394 and pathogenicity (Figure 8 and 9). All results from our VIGS and chemical inhibitor experiments
395 are consistent with our fluorescence localization experiments. Taken together, our results therefore
396 provide evidence that BICs include a focused region of plant clathrin-mediated endocytosis for
397 internalizing cytoplasmic effectors inside living plant cells (Figure 10).

398 We report two new lines of evidence that effectors are being secreted and translocated into
399 the host cytoplasm from appressoria even before growth of primary hyphae inside host cells. First,
400 we identified an effector, Bas170, that naturally accumulates in host nuclei before visible growth
401 of primary hyphae, and it also localizes to vesicles underneath appressoria at this early time point.

402 Second, effector Pwl2:mRFP, which is not normally observed before the tip-BIC stage,
403 accumulates under appressoria that failed to penetrate after both VIGS silencing and chemical
404 inhibition of rice CME. These new findings are consistent with reports that rice cells recognize
405 and respond to *M. oryzae* before and independently of appressorial penetration (Xu et al., 1998).
406 It has been predicted that *M. oryzae* appressorial pores, a transient cell wall-less region of the
407 appressorium adjacent to the plant cuticle, might be involved in molecular communication between
408 pathogen and host before penetration (Howard and Valent, 1996). Previously, the only *M. oryzae*
409 effector that was a candidate for secretion through the appressorial pore was a presumed secondary
410 metabolite that is produced by the *AVR* gene *ACE1* encoding a hybrid polyketide synthase (PKS)
411 and nonribosomal peptide synthetase (NRPS) that is specifically expressed in the cytoplasm of
412 appressoria before and during penetration (Fudal et al., 2007; Collemare et al., 2008). Therefore,
413 our new effector localization results suggest similar exquisite staging of effector expression as
414 reported for the crucifer pathogen *Colletotrichum higginsianum*, which secretes ChEC effectors
415 under the appressorial pores and at additional invasion stages during the invasion of
416 *Arabidopsis thaliana* cells (Kleemann et al., 2012). Specifically, this fungus focally secreted
417 effectors Chec6 and Chec36 from the appressorium pore, suggesting these effectors may be
418 translocated before fungal penetration (Kleemann et al., 2012). Our results with Bas170 together
419 with ChECs and Ace1 protein localization patterns indicate that many effectors might be focally
420 secreted through appressorial pores (Fudal et al., 2007; Kleemann et al., 2012), highlighting a
421 potential role for fungal appressoria in effector delivery.

422 The effector vesicle dynamics that we report support the idea that front-loaded effector
423 translocation occurs during the early stages of host cell invasion. Specifically, tip-BIC vesicles are
424 small (~87 nm), abundant and selective in terms of sorting two cytoplasmic effectors, Bas1:eYFP
425 and Pwl2:mRFP, into different vesicles. In contrast, side-BICs contain fewer, larger, less-selective
426 vesicles that contain both Bas1:eYFP and Pwl2:mRFP. Effector vesicles observed in the cytoplasm
427 were almost uniformly found at the side-BIC stage, perhaps indicating a slow-down of the
428 mechanism for effector release from the vesicles as BICs mature. The mechanism for forming
429 vesicles may result in larger vesicles, or vesicles may fuse before releasing effectors to the
430 cytoplasm in the later BIC stages. Slowdown of the translocation system would appear consistent
431 with the loss of activity in BICs as host cells fill with IH. Front-loading effector translocation from
432 BICs would make sense because cell-to-cell movement of blast cytoplasmic effectors through

433 plasmodesmata must occur in the early stages of host cell invasion while the EIHM enclosing the
434 IH remains intact and plasmodesmata in the invaded cell remain open (Sakulkoo et al., 2018; Jones
435 et al., 2021). Active BICs are surrounded by host cytoplasm with dynamic connections to the cell
436 periphery (Khang et al., 2010) (Supplemental Movie S2), where cytoplasmic streaming would
437 rapidly disperse effectors to pit fields containing plasmodesmata. In contrast, nonBIC-associated
438 IH cells invaginate the host vacuole and grow in close proximity to the host vacuolar membrane
439 with little surrounding cytoplasm (Mochizuki et al., 2015; Jones et al., 2021). Specifically, the host
440 vacuole remains intact, but shrinks as IH grow. Both the EIHM and vacuolar membrane become
441 disrupted, indicating death of the invaded cell, around the time IH move into neighboring cells
442 (Mochizuki et al., 2015; Jones et al., 2021). However, by this time, IH have established themselves
443 in living neighboring cells.

444 There is evidence supporting occurrence of clathrin-mediated endocytosis at the EHM in
445 one additional pathosystem. That is, transmission electron micrographs of the interfacial matrix
446 between the intracellular hyphae [called monokaryotic (M)-haustoria] of the monokaryotic rust
447 fungus *Uromyces vignae* and its host cowpea (*Vigna unguiculata*) shows clathrin-coated pits
448 (diameter ca. 50-70nm) on the EHM at M-haustoria hyphal tips that contained dense cytoplasm
449 and were presumably growing (Stark-Urnau and Mendgen, 1995). The coated vesicles were
450 labeled by an antibody recognizing the heavy chain subunit of clathrin. Long tubules extending
451 into the host cytoplasm, as well as coated vesicles in the surrounding host cytoplasm, were also
452 labeled with the antibody, indicating that endocytosis occurs at the EHM (Stark-Urnau and
453 Mendgen, 1995; O'Connell and Panstruga, 2006). It was suggested that these endocytic vesicles
454 might be involved in effector uptake into host cells in addition to membrane recycling from host
455 exocytosis. Unfortunately, lack of transformation capability and identification of effectors makes
456 it difficult to follow up on these intriguing results with *U. vignae*. Additional TEM studies support
457 our results that transient silencing of lipid raft-mediated endocytosis component Flotilin1, as well
458 as filipin treatment, had little effect on BIC structure and effector vesicle formation. Freeze-
459 fracture transmission electron microscopy (TEM) following filipin treatment revealed an absence
460 of granular filipin-sterol complexes on the EHM of two rust fungi, *Puccinia coronata* and
461 *Uromyces appendiculatus* (Harder and Mendgen, 1982), suggesting that the extrahaustorial
462 membrane contains less sterol than normal plasma membranes, indicating that the EHM appears
463 depleted in sterol-rich lipid rafts.

464 Differences in infection strategies among various filamentous biotrophic or hemibiotrophic
465 pathogens would be consistent with use of different strategies for effector translocation in different
466 pathosystems. A recent report indicates that a complex of seven proteins from the smut pathogen
467 *U. maydis* is critical for infection and implicated in translocation of cytoplasmic effectors into
468 maize cells (Ludwig et al., 2021). This basidiomycete fungus colonizes host tissue as intracellular
469 hyphae that pass through and between host cells without obviously specialized interfacial zones,
470 and fluorescent fusion proteins of cytoplasmic effectors have not been visualized in the host cell
471 cytoplasm in this pathosystem (Lo Presti et al., 2017). *U. maydis* produces galls on maize seedlings
472 and grows systemically as the plant grows to finally invade ovaries, which swell into dramatic
473 sporulating galls. In contrast, *M. oryzae* densely colonizes a localized tissue area that will become
474 a visible eyespot lesion that releases spores to reinitiate the infection cycle within 7 days. Different
475 pathogenic lifestyles could have different demands for cytoplasmic effector translocation.
476 Taken together, our data strongly suggest that clathrin-mediated endocytosis occurring in
477 BICs is a key mechanism for internalization of *M. oryzae* effectors inside living rice cells,
478 beginning even before appressorium penetration on the host surface. Important unknowns for
479 future study include the molecular mechanisms of how the endocytic machinery interacts with
480 effector cargos (Qi et al., 2018), including how different effectors are sorted out into different
481 vesicles as shown in Figure 2. It is important to understand vesicle dynamics through time and
482 why effector vesicles become larger and less selective as BICs mature. It is important to understand
483 if, and if so, how, Bas83 contributes to membrane recruitment to BICs and the EIHM surrounding
484 BIC-associated cells. It is unknown how the effector vesicles are disrupted, releasing effectors
485 into the rice cytoplasm and how various effectors are then targeted to their destinations in host
486 cells including, in some cases, movement through plasmodesmata into neighboring host cells. It is
487 also important to understand the role for appressoria in effector secretion before penetration, and
488 how these early effectors, such as the host nuclear localized effector Bas170, function to promote
489 infection. Finally, it is critical to translate molecular mechanisms of blast biotrophic invasion into
490 strategies for controlling devastating diseases on rice, wheat and other food crops worldwide.
491

492 **METHODS**

493 **Live-cell imaging of *M. oryzae* effectors *in planta***

494 Fungal strains were stored in dried filter papers at -20˚C, and cultured on rice polish agar plates at
495 25˚C under continuous light for 2 weeks (Valent and Chumley, 1991). Rice sheath inoculations
496 were performed as described (Kankanala et al., 2007). The susceptible rice variety YT-16 was
497 used unless mentioned otherwise. Briefly, 7-cm-long sheath pieces from 3-week-old plants were
498 placed in a sealable Pyrex glass moist chamber. Leaf sheath sections were placed on inverted 8-
499 well PCR tube strips to avoid contact with wet paper and to hold epidermal cells directly above
500 the mid-vein horizontally flat for uniform inoculum distribution in the trimmed sheath pieces. A
501 spore suspension ($10^4$ spores/ml in sterile 0.25% gelatin, Cat. #G-6650, Sigma-Aldrich) was
502 prepared from 10-day old cultures and was injected into one end of the sheath using a 100-ml
503 pipette. Each segment was trimmed at 18–30 h.p.i., treated with specific dyes or inhibitors, or
504 imaged immediately by laser confocal microscopy. Confocal imaging was performed with a Zeiss
505 LSM780 confocal microscope system using two water immersion objectives, C-Apochromat
506 40x/1.2 WCorr. and C-Apochromat 63x/1.2WCorr. Excitation/emission wavelengths were 488
507 nm/505–550 nm for eGFP and FM1-43, and 543 nm/560–615 nm for mRFP, mCherry, Phalloidin
508 and FM4-64. Images were acquired and processed using Zeiss ZEN 2010 software. Images of
509 effector vesicles in Figure 3C were obtained using a Leica SP8 confocal microscope system with
510 a water immersion objective HC PL APO 63x/1.20 WCorr. Excitation/emission wavelengths were
511 488 nm/505–550 nm for eGFP and 543 nm/560–615 nm for mRFP.

512 **Fungal strains, DNA manipulation, and fungal transformation**

513 *Magnaporthe oryzae* wild type strain Guy11, a field isolate from rice in French Guiana, was
514 obtained from J.L. Notteghem (Centre de Cooperation Internationale en Recherche Agronomique
515 pour le Developpment). *M. oryzae* transformants are described in Supplemental Table S1 online.
516 Effector:mRFP and Effector:eGFP expression plasmids were constructed by PCR amplifying
517 different effector gene regions and fusing them to the N-terminus of mRFP and eGFP, respectively.
518 Details of construction of each plasmid are described in Supplemental Table S2, and primers are
519 listed in Supplemental Table S3. For all fusion constructs, transcriptional and translational fusions
520 were verified by DNA sequencing. See Supplemental Table S2 online for plasmids used, and
521 Supplemental Table S3 for PCR primers used. Plasmids were transformed into laboratory strain
522 Guy11 (Leung et al., 1988) using *Agrobacterium tumefaciens*–mediated transformation (Khang et
523 al., 2006). In several cases, two fluorescently labelled effectors were introduced by co-
524 transformation with separate plasmids (Sweigard et al., 1995). Because positive transformants

525 showed similar fluorescence patterns with varying intensities, those with strongest fluorescence
526 were studied (see Supplemental Table S1 online). For each construct cloned in *M. oryzae*, at least
527 two independent transformants showing identical phenotypes to the wild type were selected and
528 assayed together.

529 **Targeted deletion of Bas83 gene**

530 *Split-marker recombination method for Bas83 gene knockout via protoplast transformation*:
531 Targeted gene replacement mutation of the *M. oryzae Bas83* gene was attempted using the split
532 marker strategy as modified by Kershaw and Talbot (2009). Gene replacement was performed by
533 replacing the 606-bp *Bas83* locus with a hygromycin resistance selectable marker, encoding a 1.4-
534 kb hygromycin phosphotransferase (*HPH*) resistance cassette (Carroll et al., 1994). The two
535 overlapping segments of the *HPH* templates were PCR amplified using primers M13F with HY
536 and M13R with YG (Catlett et al., 2003) (see Supplemental Table S3 online) as described
537 previously (Kershaw and Talbot, 2009). One-kb DNA fragments upstream and downstream of the
538 *Bas83* open reading frame were generated using the primers Bas83LF-F and Bas83LFHY-R and
539 Bas83RFYG-F and Bas83RF-R amplified from genomic DNA of the Guy11 strain. A second-
540 round PCR reaction was performed to fuse the overlapping split hph marker templates with the
541 left and right flanking regions of the Bas83 locus. Wild-type *M. oryzae* strain Guy11 was then
542 transformed with the deletion cassettes (2 μg of each flank). Putative transformants were selected
543 in the presence of hygromycin B (200 μg/ml) and analyzed by PCR using the primers
544 Bas83:BASKOtest-F and Bas83:BASKOtest-R (Supplemental Table S3; Supplemental Figure
545 S5). This assay was repeated three times. Gene sequences on either side of *Bas83* were retrieved
546 from the NCBI database (https://www.ncbi.nlm.nih.gov/).

547 *Attempted Bas83 deletion via Agrobacterium-mediated transformation*: For gene
548 replacement transformation, cassettes were constructed by amplifying ~1.0 kb of 5′- and 3′-
549 flanking regions for each predicted coding sequence. The *HPH* gene (Carroll et al., 1994) was
550 cloned between the two flanking regions using a fusion PCR strategy. The three pieces together
551 were cloned first into the pJET1.6 vector (Invitrogen) for sequence analysis and later into binary
552 vector pGKO2 (Addgene: Plasmid #63617; Khang et al., 2005) using a restriction ligation strategy.
553 *M. oryzae* KU70 and KU80 spores were transformed using *A. tumefaciens* (Khang et al., 2005)
554 strains AGL1 and EHA105 (Hellens et al., 2000). After two rounds of selection in TB3 media
555 containing 200 μg/mL of hygromycin, 400 independent fungal transformants were analyzed for

556 gene replacement events by PCR amplification using the primers Bas83:BASKOtest-F and
557 Bas83:BASKOtest-R (Supplemental Figure S5). This assay was repeated three times.

558 **Staining with FM 4-64, FM 1-43, and Rhodamine Phalloidin, and treatment with**
559 **pharmacological inhibitors**

560 To examine membrane dynamics at the BIC, rice sheaths (cv. YT16) were inoculated with *M.*
561 *oryzae* transformants expressing fluorescently-labeled effectors ($2x10^4$ spores/ml in 0.25% gelatin
562 solution) and incubated for 20-26 hours at 25˚C for subsequent FM-dye treatment. Infected rice
563 sheaths were treated with FM 4-64 or FM 1-43 (4 mg/ml in water). An aqueous 17mM stock
564 solution of FM 4-64 (Cat #13320, Invitrogen, Carlsbad, CA) and FM 1-43 (Cat # T3163,
565 Invitrogen, Carlsbad, CA) were prepared and stored at -20˚C as described (45). *In planta*,
566 inoculated leaf sheaths, 24 h.p.i., were trimmed into ultrathin sections (2-3 layers of cells; 10 x 10
567 mm) and incubated in a 10-mM aqueous working solution for 3–5 hours. Leaf sheaf sections were
568 subsequently transferred to ultrapure water and incubated for 20 min (25 ˚C) to remove excess
569 dyes for uniform membrane staining. For *in planta* experiments with Rhodamine Phalloidin (Cat#
570 R415, ThermoFisher Scientific), we prepared working solutions of 66 µM in 0.1% DMSO and
571 treated the inoculated tissue as described for FM dyes.

572 To examine the effects of endocytosis inhibitors on *in planta* effector uptake, inoculated
573 trimmed rice sheaths were incubated at 25˚C with Methyl-β-cyclodextrin (20 mM), or
574 Chlorpromazine (10 µg/mL), or Cantharidin (25 mM), or Fluazinam (20 mM), or Triclosan
575 (20mM), or Wortmannin (20 nM), or Concanamycin A (50 mM) (all from Sigma) solution for 1-
576 5 hours. Negative controls were performed with ultrapure water (Methyl-β-cyclodextrin,
577 Chlorpromazine, and Fluazinam) or 0.1% DMSO (Cantharidin, Filipin and Wortamanin) (see
578 Table 1).

579 **Generation of transgenic rice plants**

580 Production of transgenic plants expressing the plant plasma membrane marker low-temperature
581 inducible protein 6B, LTi6B:GFP was previously described (Mentlak et al., 2012; Giraldo et al.,
582 2013). Transformants of rice cultivar Sasanishiki expressing LifeAct:eGFP were generated in the
583 laboratory of NJT. Expression plasmids for CME and CIE marker genes were constructed by PCR
584 amplifying the marker gene regions and fusing them to the N-terminus of eGFP. The *CLC1* gene
585 was amplified from genomic DNA of YT16 rice using the primers KpnI_OsCLC1Prom1-F1 and

586 XhoI_OsCLC1-R1. The PCR product was digested with *Kpn*I and *Xho*I and integrated into
587 pSH1.6EGFP (Plasmid #42323, Addgene). The *Flot1* gene was amplified from genomic DNA
588 from YT16 rice using the primers HindIII_OsFlot1Prom1-F1 and Eco47III_OsFlot-R1. The PCR
589 product was digested with *Hind*III and *Eco*47III and integrated into pSH1.6EGFP. CLC1:eGFP
590 was amplified from pSH1.6_CLC1:eGFP using the primers CACC_OsCLC1-F1 and eGFPT2-R2,
591 and cloned into pENTR (pENTR™/D-TOPO™ Cloning Kit, ThermoFisher Scientific) following
592 the manufacturer's protocol. Flot1:eGFP was amplified form pSH1.6_Flot1:eGFP using the
593 primers CACC_OsFlot1-F1 and eGFPT2-R2, and cloned into pENTR following manufacturer's
594 protocols. Endocytosis marker:eGFP construct were cloned into the *Agrobacterium* vector
595 pIPKb001 (Himmelbach et al., 2007) using the Gateway LR Clonase II kit (Invitrogen) following
596 the manufacturer's protocol. All the fusion constructs had transcriptional and translational fusions
597 verified by DNA sequencing. Gene fusions for expressing the rice endocytosis markers
598 CLC1:eGFP (CME) and Flot1:eGFP (CIE) under their native promoters were introduced into
599 *Agrobacterium tumefaciens* EHA105 using the freeze-thaw method (Holsters et al., 1978). Mature
600 seed-derived callus from rice (*Oryza sativa L. Japonica*) cv. YT16 was used for *Agrobacterium*-
601 mediated transformation (Park et al., 2001). After inoculating with *A. tumefaciens*, callus was
602 transferred to regeneration medium for 4-10 weeks at 25˚C under a 16-h photoperiod. The
603 regenerated shoots were transferred to rooting medium for four more weeks, then established in
604 soil. Putative transformants of rice were selected on 100 µg/ml hygromycin, and expression
605 checked by qRT–PCR and epifluorescence microscopy.

606 **Silencing of rice genes**

607 In order to evaluate the role of plant endocytosis on disease development and effector uptake, we
608 performed VIGS using the Brome mosaic virus system developed by R.S. Nelson (Noble
609 Foundation, Ardmore, OK). We targeted *AP-2α*, *CHC1* (CME) and *Flot1* (CIE) mRNA in rice
610 plants (cultivar IR64) undergoing infection. The target rice sequences were cloned in the pC13/F3-
611 13m VIGS vector as described (Ding et al., 2006; Ding et al., 2007) and subsequently sequenced
612 to verify sequence accuracy. RNA transcripts were synthesized from the final VIGS vector. An
613 empty vector pC13/F3-13m was used as negative control. The final infectious transcripts of
614 pC13/F3-13m / AP-2α, pC13/F3-13m / CHC1, pC13/F3-13m /Flot1 and pC13/F3-13m (a control
615 virus without an insert) were inoculated with pC13/F1+2 in 7 to 10 day old IR64 rice plants
616 according protocols described by Ding et al (2006). Knockdown of the target genes was confirmed

617 by qRT-PCR at 15 days post inoculation. At this point, rice plants showing satisfactory reduction
618 of the transcription levels were used in our standard conidial spray inoculation and leaf sheath
619 assays with fungal strains expressing fluorescently-labeled effectors.

620 **Statistics**

621 All experiments were performed in triplicate and repeated three times. Calculations (unpaired t
622 test, analysis of variance) were performed with the software XLSTAT version 2009.4.02
623 (Addinsoft).

624

625 **ACKNOWLEDGEMENTS**

626 We acknowledge and thank Rick Nelson (Noble Foundation, Ardmore, OK) for providing the
627 VIGS vectors and hosting E.O.-G. in his laboratory to learn the VIGS assay. We thank the Talbot
628 laboratory for assistance and hospitality during a working visit for E.O.-G at the University of
629 Exeter. We thank Hiromasa Saitoh (Iwate Biotechnology Research Center, Kitakami, Iwate,
630 Japan) and Ryohei Terauchi (Iwate Biotechnology Research Center, Kitakami, Iwate, and Kyoto
631 University, Japan) for sharing transgenic rice expressing plant plasma membrane marker
632 LTi6B:GFP. This project was supported by Agriculture and Food Research Initiative Competitive
633 Grant no. #2017-67013-26525 from the USDA National Institute of Food and Agriculture Plant
634 Biotic Interactions program. This is Contribution no. 22-053-J from the Kansas Agricultural
635 Experiment Station.

636

637 **AUTHOR CONTRIBUTIONS**

638 E.O.-G. and B.V. designed experiments and analyzed data: E.O.-G. performed most of the
639 research. T.M.T., J.P. and S.P. produced and analyzed transgenic rice lines expressing the rice
640 CLC1:eGFP and Flot1:eGFP fluorescent fusion protein genes. M.D., M.M.-U., C.R.H. and A.H.V.
641 assisted with microscopy and Bas83 Knockout experiments and general laboratory experiments;
642 N.J.T. provided transgenic rice lines expressing LTi6B:GFP and LifeACT:GFP; E.O.-G., B.V. and
643 N.J.T wrote and edited the article.

644

645 **Table 1. Chemical inhibitors of endocytosis**

| Chemical | Target | Mode of action | Comments | References |
|---|---|---|---|---|
| Filipin | CIE* | Binds to sterols in the membrane. | Toxic at higher concentrations. | (Rodal et al., 1999) |
| Methyl-β-cyclodextrin | CIE | Deplete cellular membranes of sterols by increasing the water solubility of the sterol. | caveolae-dependent endocytosis. | (Rodal et al., 1999) |
| Chlorpromazine | CME** | Translocates clathrin and AP2 from the cell surface to intracellular endosomes. | Also inhibits CIE in some cells. | (Wang et al., 1993) |
| Cantharidin | CME | Inhibits PP2A (protein phosphatase 2A) | Affects flg22-mediated FLS2 endocytosis. | (Serrano et al., 2007) |
| Triclosan | CME | Inhibits PP2A (protein phosphatase 2A) | Affects flg22-mediated FLS2 endocytosis. | (Serrano et al., 2007) |
| Wortmannin | nd*** | Inhibits PI3Ks, blocks late trafficking to the vacuole, multivesicular bodies and endocytosis. | Late endosomes lose their clathrin; Potential CME association. | (Bright et al., 2001; Sachse et al., 2002; Robinson et al., 2008) |
| Concanamycin A | nd | Targets V-type ATPase and blocks trafficking at trans-Golgi network, endosome acidification. | Induces acidification crucial for endocytic pathways. | (Maranda et al., 2001; Robinson et al., 2008) |

646 *CIE: clathrin-independent endocytosis; **CME: clathrin-mediated endocytosis; ***nd: not determined.

647

648 Figure 1

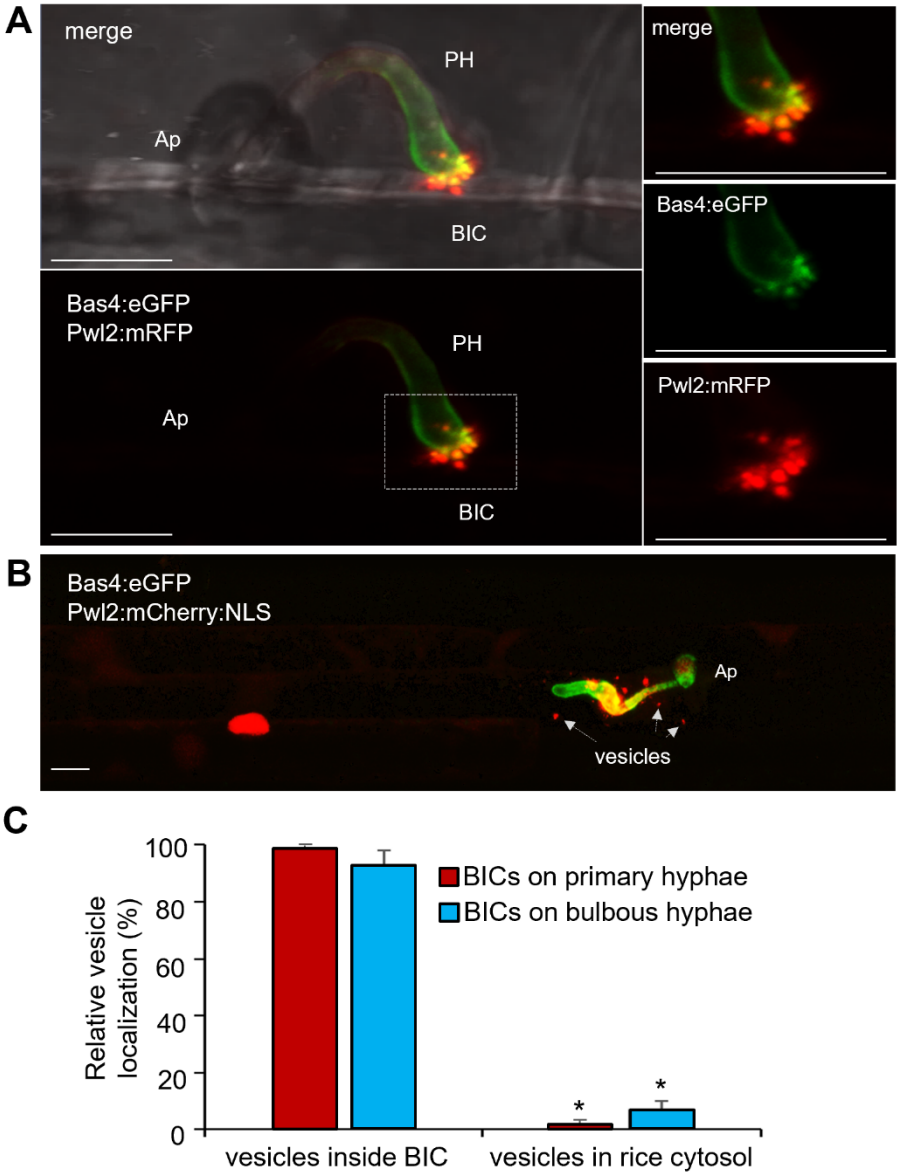


649
650 **Figure 1**. **BIC vesicular organization and effector vesicles in the rice cell cytoplasm**. **A.**
651 Cytoplasmic effector-labeled vesicles in a tip-BIC of strain KV217 expressing Pwl2:mRFP and
652 Bas4:eGFP at 17 hpi. The appressorium (Ap) and the first half of the primary hypha (PH) are
653 shown out of focus. Separate mRFP and eGFP channels (right) for the inset show the base layer
654 of apoplastic effector Bas4:eGFP and the outer vesicular layer labeled by cytoplasmic effector
655 Pwl2:mRFP. **B.** A side-BIC shown above the bulbous IH of strain KV168 expressing
656 Pwl2:mCherry:NLS and Bas4:eGFP at 24 hpi. Effector vesicles in are visible in the host cytoplasm
657 at a distance from the BIC. The Bas4:eGFP control shows that the EIHM surrounding the IH
658 remains intact. Addition of an artificial NLS to the fluorescent Pwl2 fusion protein facilitates
659 visualization of effector translocation and accumulation inside the host cell nucleus. **C.**

660 Quantification of the relative localization of cytoplasmic effector vesicles, assessed using strain
661 KV217 (same as in panel A) at 98 infection sites for each BIC developmental stage; three
662 biological replicates. Bars in C represent standard deviation. *P≤0.05. Images in A and B (merged
663 bright field, eGFP and mRFP fluorescence) are shown as projections of confocal optical sections.
664 Bars = 10 μm.
665

666 Figure 2

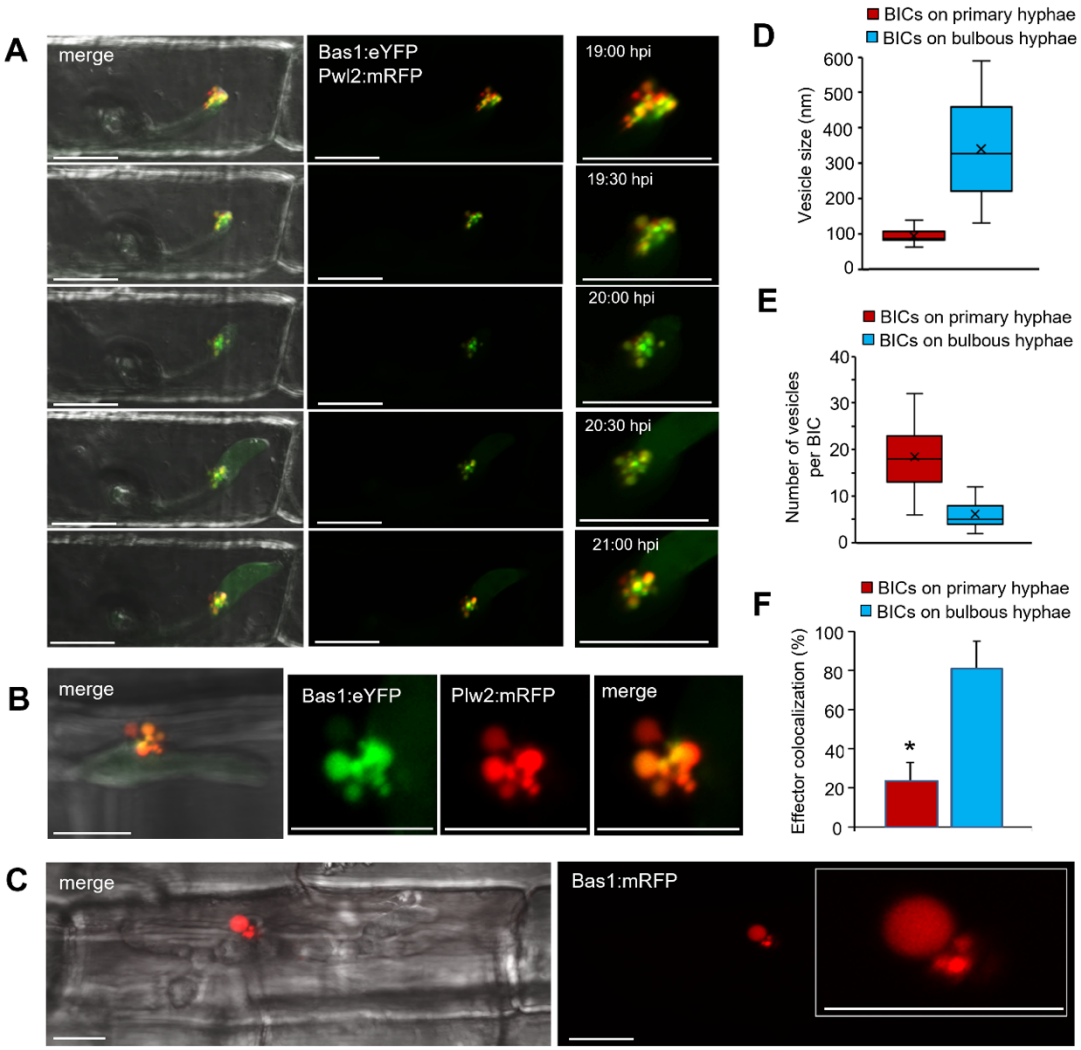


667

668 **Figure 2. Dynamics of BICs and effector vesicles during differentiation of primary hyphae**
669 **to first bulbous invasive hyphae. A.** Dynamics of two cytoplasmic effectors, Pwl2:mRFP and
670 Bas1:eYFP (Strain KV211), as a tip-BIC (top panel) becomes a side-BIC (bottom panel), imaged
671 every 30 min from 19 to 21 hpi. Images (left to right) are merged bright field, eYFP and mRFP
672 fluorescence at 5 time points; merged eYFP and mRFP at same time points in both the same and
673 enlarged views of the fluorescent BICs shown as projections of confocal optical sections. Bars =
674 10 µm. **B.** Cytoplasmic effectors Pwl2:mRFP and Bas1:eYFP (Strain KV211) co-localize in larger
675 vesicles in a side-BIC at 24 hpi. **C.** A rare extremely large effector vesicle (diameter 3.9 µm) in a
676 late stage side-BIC formed by strain KV170 expressing cytoplasmic effector Bas1:mRFP in a rice
677 cell at 30 hpi. **D,E.** Box and whisker plots comparing vesicle sizes (D) and number of vesicles (E)
678 in tip- and side-BICs formed by strain KV211 invading rice cells. **F.** Bar chart showing
679 quantification of Bas1:eYFP and Pwl2:mRFP colocalization (KV211) in vesicles in tip- and side-
680 BICs. Bars in F are standard deviations. *$P \leq 0.05$; three times 100 BICs observed in D-F.

681 Figure 3

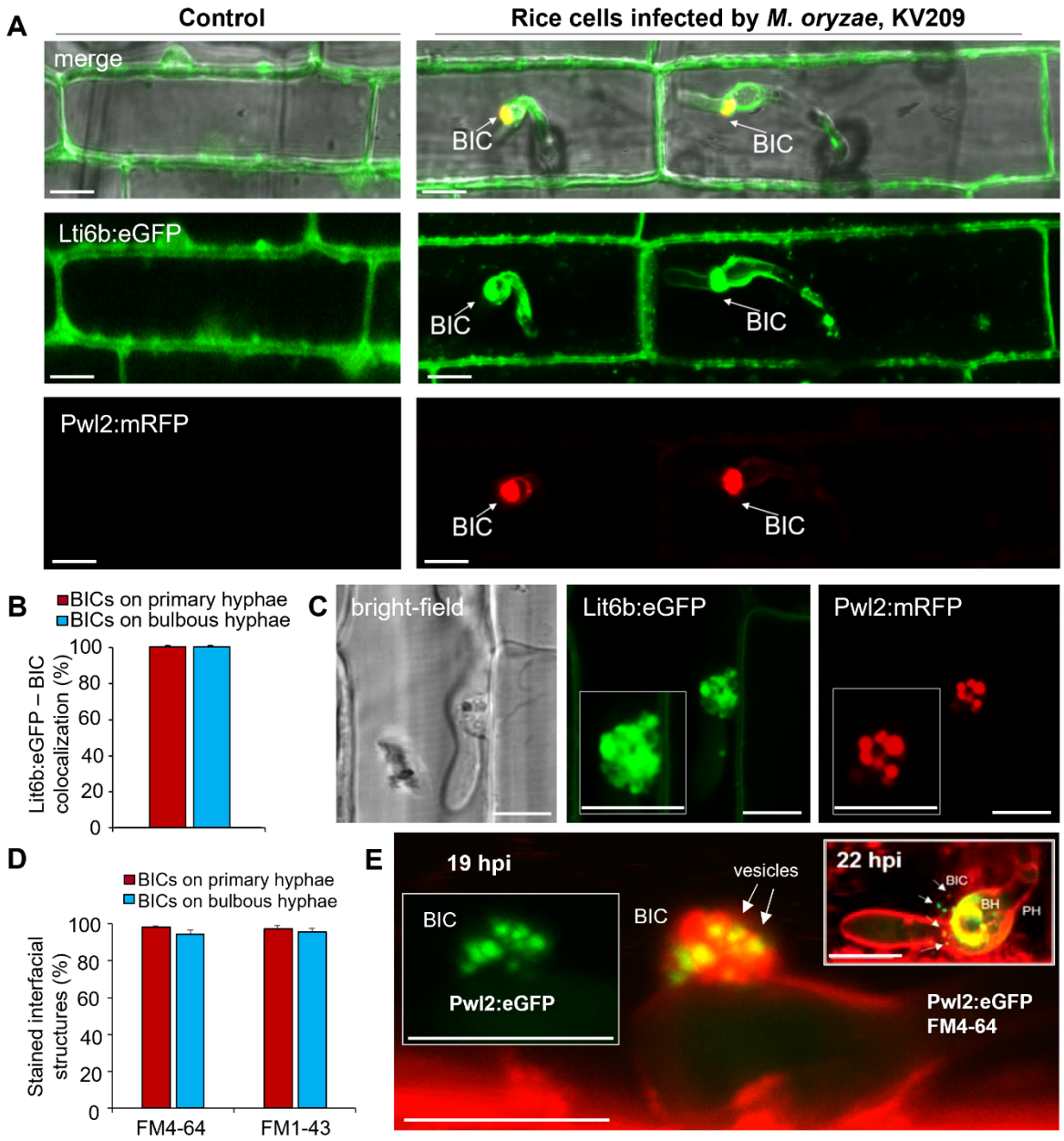


682

683 **Figure 3. Effector vesicles are derived from plant plasma membrane. A.** Rice expressing
684 plasma membrane marker LTi6b:eGFP in non-infected cells (left column) and in cells infected by
685 strain KV209 expressing Pwl2:mRFP (right column). Colocalization confirms BICs as plant
686 plasma membrane-rich structure. **B.** Quantification of the colocalization of LTi6b:eGFP with BICs
687 at both developmental stages. Three times 90 infection sites observed. **C.** Localization assays of
688 LTi6b:eGFP relative to Pwl2:mRFP in an infected rice cell at 22 hpi showing LTi6b:eGFP
689 outlining vesicles in the BIC. Insets show BIC vesicles at higher magnification. Bars are 10 µm.
690 **D.** Quantification of BICs stained by the endocytosis tracer dyes FM 4-64 and FM 1-43 at the tips
691 of primary hyphae and beside the first bulbous IH. Three times 90 infection sites observed
692 treatment. **E.** Colocalization of BIC effector vesicles and FM4-64-stained membranes in BICs.

693 Images of strain KV176 expressing Pwl2:eGFP in BICs beside the first bulbous IH cell in rice
694 stained with FM4-64 and observed at 19 hpi. The image is merged eGFP and FM 4-64 fluorescence
695 with eGFP fluorescence shown alone in the inset in the lower left. The upper right inset shows a
696 top-down view of a different BIC, shown below the image plane, at 22 hpi. Inset arrows indicate
697 Pwl2:eGFP vesicles near the BIC. Images are projections of confocal optical sections. Bar = 10
698 µm. See Supplemental Movie S2 for yet another side-BIC with additional examples of
699 colocalization of FM 4-64 fluorescence and Pwl2:eGFP.

700

701 Figure 4

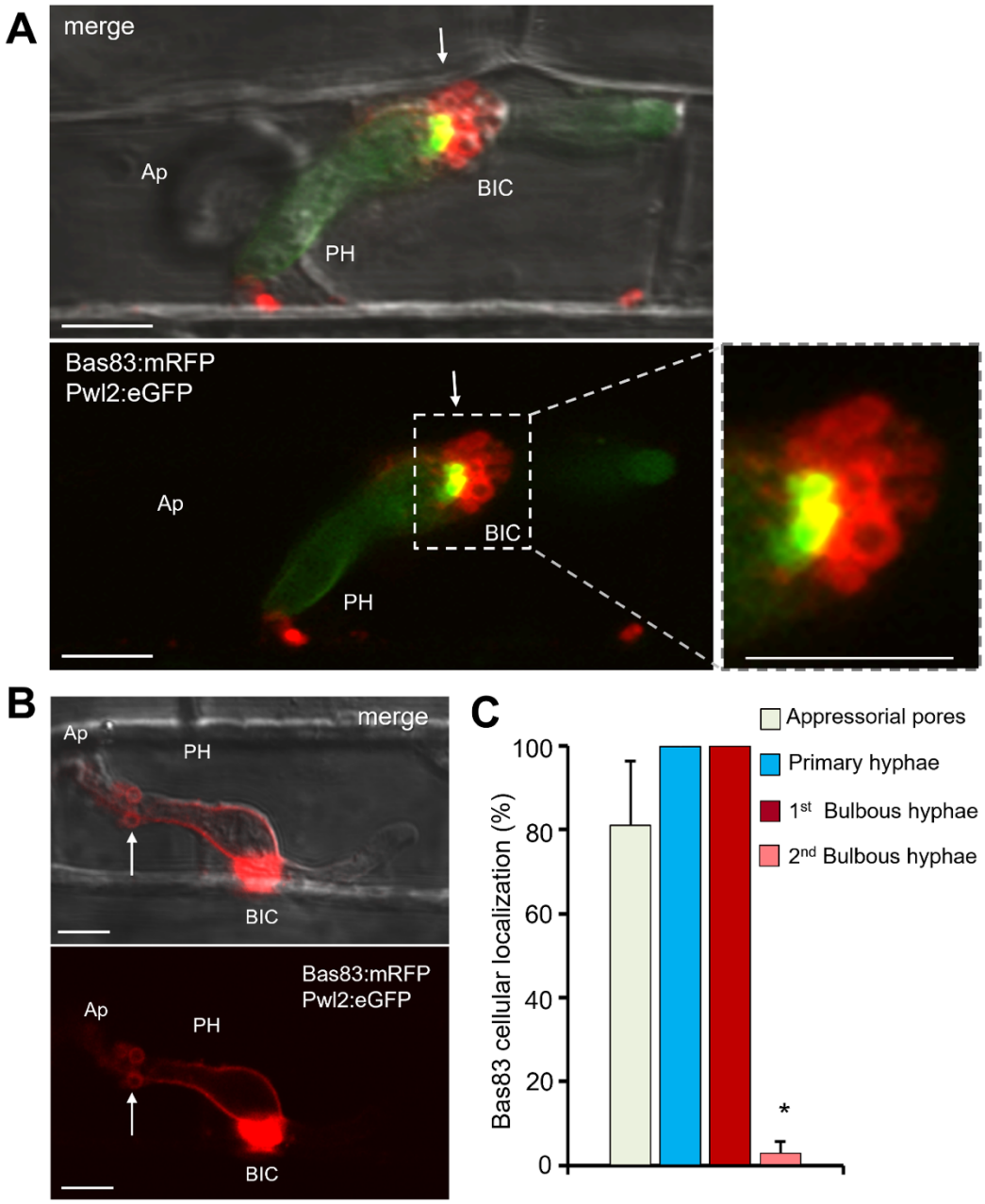


702

703 **Figure 4. Bas83 is a novel effector associated membrane vesicles surrounding BICs and BIC-**
704 **associated cells. A.** Bas83:mRFP binds apparent membrane vesicles surrounding a side-BIC
705 (white arrow) labeled with Pwl2:eGFP (strain KV222). **B.** Bas83:mRFP (KV220) binds to bubble-
706 like structures near a primary hypha (arrow) as well as labeling a BIC and outlining BIC-associated
707 cells. Images (merged bright field, eGFP and mRFP fluorescence) are projections of confocal
708 optical sections. See additional images in **Supplemental Figure S3**. Bars = 10 µm. **C.**
709 Quantification of the cellular localization of Bas83:mRFP during biotrophic invasion of *M. oryzae*
710 (KV220). Bars are standard deviations. *$P \leq 0.05$; three times 100 infection sites observed per
711 experiment.

712 Figure 5

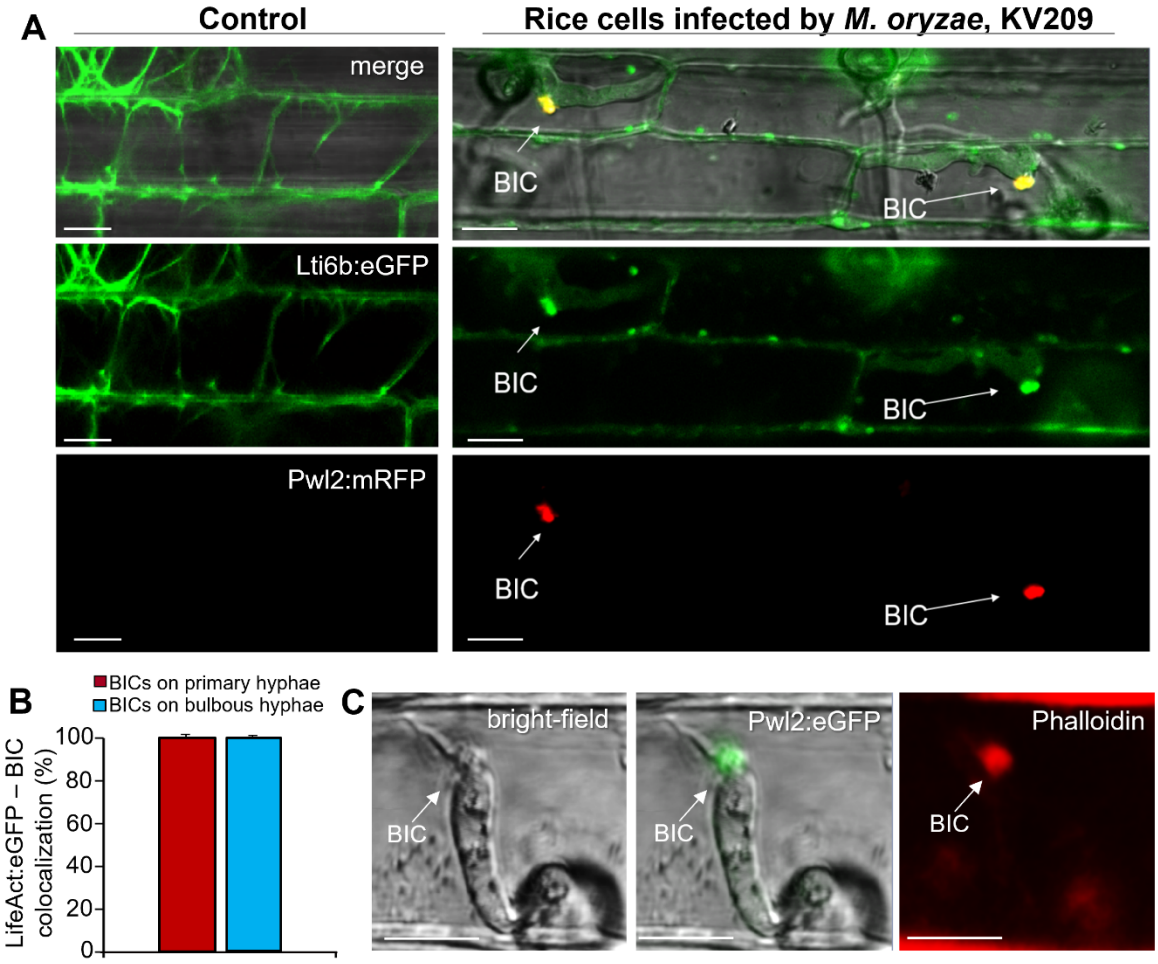


713
714

715 **Figure 5. BICs contain plant actin. A.** Rice LifeAct:eGFP localization during biotrophic invasion
716 by *M. oryzae*. A rice line expressing LifeAct:eGFP in non-infected cells (left column) and cells
717 infected by *M. oryzae* strain KV209 expressing Pwl2:mRFP in BICs (right column).
718 Colocalization shows BICs are rich in plant actin. **B.** Quantification of the colocalization of
719 LifeAct:eGFP with both tip- and side-BICs. Three times 100 infection sites observed. **C.**
720 Rhodamine phalloidin conjugate (red fluorescence staining actin filaments) colocalizes with
721 Pwl2:eGFP in rice cells infected by strain KV176, confirming the actin-rich structure of the BIC.
722

723 Figure 6

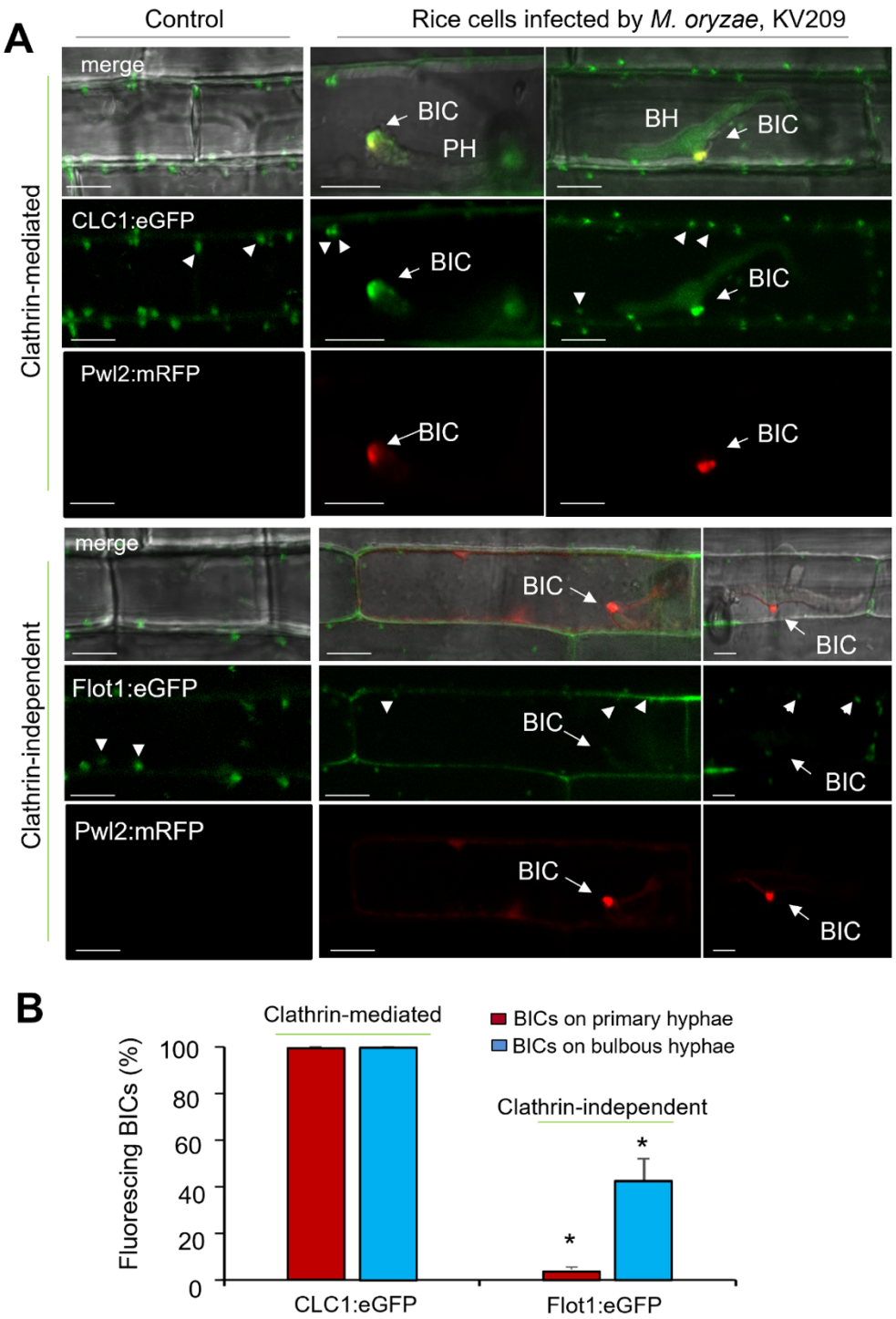


724
725 **Figure 6. BICs uniformly contain clathrin, but not in flotillin1. A.** Rice leaf sheaths expressing
726 OsCLC1:eGFP (top panels) or OsFlot1:eGFP (bottom panels) were inoculated with strain KV209
727 expressing Pwl2:mRFP. Shown from left to right are a non-infected rice sheath cell; an infected
728 cell containing a primary hypha (PH) with a tip-BIC at 19 hpi; and an infected cell containing a

729 bulbous IH (BH) with a BIC at 22 hpi. Arrowheads indicate endocytic foci and arrows indicate
730 BICs. Bars=10μm. **B.** Quantification of the colocalization of OsCLC1:eGFP or OsFlot1:eGFP
731 with BICs on the tip of a primary hypha and beside the first bulbous IH cell. Bars are standard
732 deviations. *$P \leq 0.05$; three times 97 BICs observed each treatment.
733

734 Figure 7

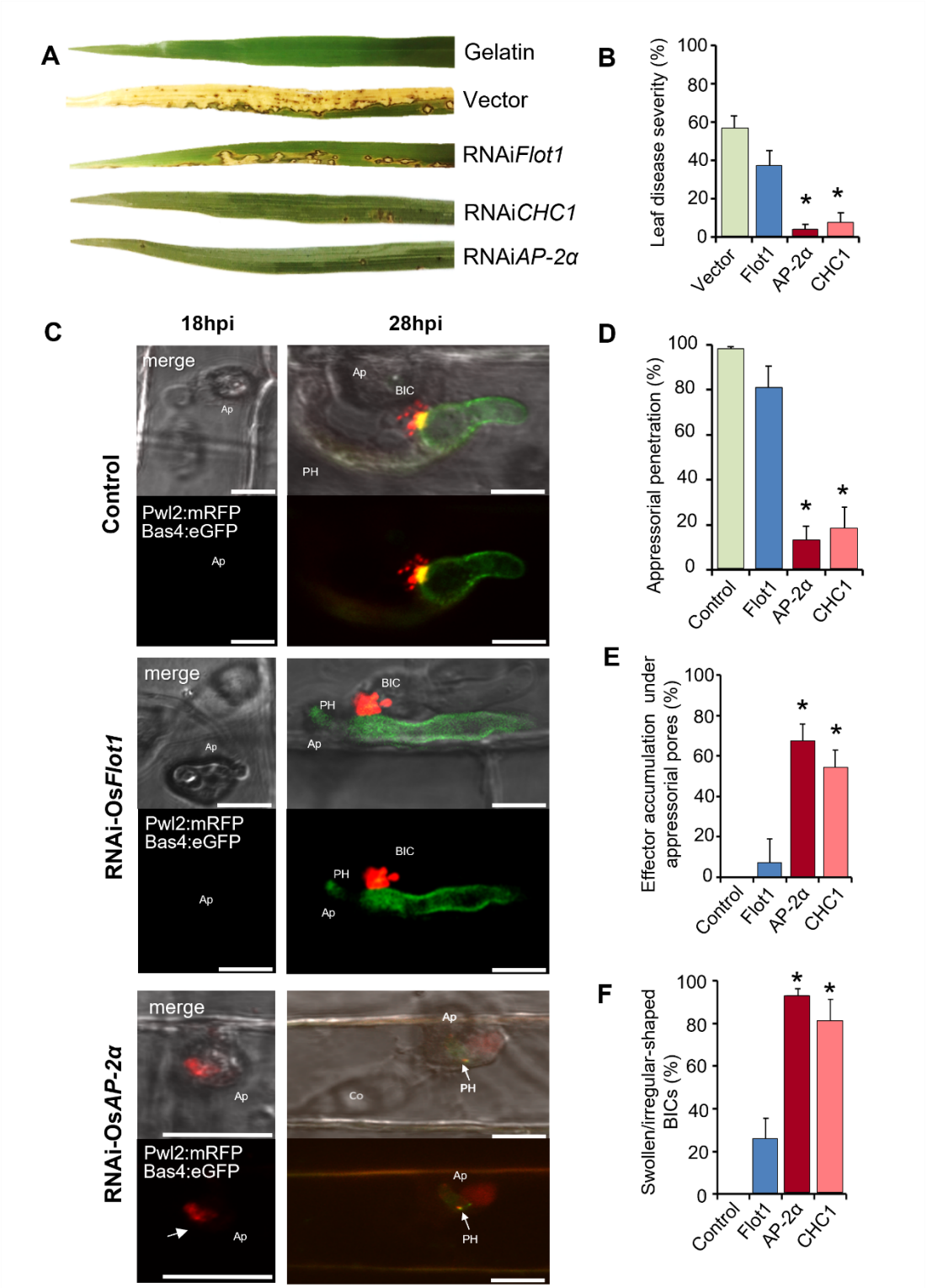


735

736 **Figure 7. Silencing of rice endocytic machinery suggests roles in pathogenicity and fungal**
737 **effector translocation. A.** Disease severity in rice leaves, cultivar IR64, undergoing silencing of
738 rice endocytic genes**.** Whereas silencing of *Flot1* gene showed minor effects on pathogenesis, the

739 silencing of the key clathrin-mediated endocytosis genes, *AP-2*α and CHC1 resulted in a
740 significant reduction in pathogenicity in whole plant spray inoculation assays. **B.** Quantification
741 of diseased area in rice expressing RNAi*AP-2*α, RNAi*CHC1*, RNAi*Flot1* or empty vector infected
742 by *M. oryzae* strain Guy11 (P≤0.05 for all treatments; n = 9 rice plants for each treatment; mean +
743 standard deviation, three experiments). **C.** Effects of silencing rice endocytosis genes on the
744 localization of Pwl2:mRFP and Bas4:eGFP during biotrophic invasion of *M. oryzae* (KV217).
745 Wild type IR64 rice and rice expressing RNAi*Flot1* or RNAi*AP-2*α were infected by KV217
746 expressing Pwl2:mRFP and Bas4:eGFP at 26 hpi. Note the accumulation of Pwl2:mRFP under the
747 appressorium (Ap) and the pale Bas4:eGFP fluorescence associated with the short primary hypha
748 (PH) in the RNAi*AP2*α rice compared to the control and RNAi*Flot1* rice. BICs formed in
749 RNAi*AP-2*α and RNAi*CHC1* rice show similar swollen phenotype. Images in C (merged bright
750 field, eGFP and mRFP fluorescence) are shown as projections of confocal optical sections. Bars =
751 10 µm. **D-F.** Quantification of the effector accumulation under appressoria (D), appressorial
752 penetration (E), and swollen, irregular BICs (F) in rice expressing RNAi*Flot1* and RNAi*AP-2*α,
753 RNAi*CHC1* and empty vector infected by *M. oryzae* strain KV209 expressing Pwl2:mRFP at 26
754 hpi. Bars are standard deviations, three experiments. (*P≤0.05; three times 100 infection sites
755 counted each treatment).
756

757 Figure 8

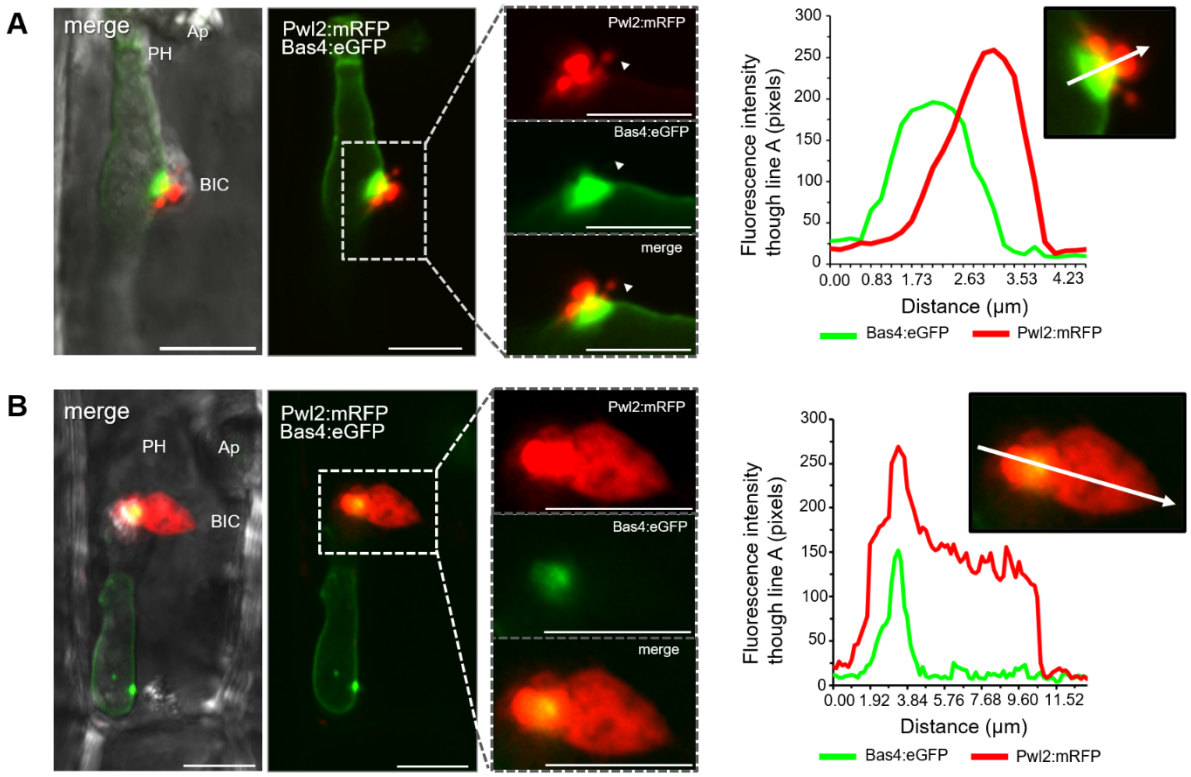


758

759 **Figure 8. Treatment with CME inhibitor cantharidin impacts the localization of cytoplasmic**
760 **effector Pwl2, but not apoplastic effector Bas4. A.** Apoplastic effector Bas4:eGFP identifies an
761 inner base layer of the BIC relative to cytoplasmic Pwl2:mRFP, as shown by fluorescence intensity
762 linescans for GFP (green) and mRFP (red) along the path of the white arrow. This side-BIC was
763 formed during invasion of rice by strain KV217 expressing Pwl2:mRFP and Bas4:eGFP at 26 hpi.
764 **B.** After treatment with CME inhibitor cantharidin, localization of Bas4:eGFP in the BIC base
765 appears unaffected, compared to the non-vesicular swollen localization of Pwl2:mRFP, as shown
766 by fluorescence intensity linescans for GFP (green) and mRFP (red) along the path of the white
767 arrow. Note linescan distance is almost 3-fold greater after cantharidin treatment. This BIC was
768 formed by KV217 at 26 hpi, as in control panel A. Images (merged bright field, eGFP and mRFP
769 fluorescence) are shown as projections of confocal optical sections. Appressorium (Ap); Primary
770 hypha (PH). Bars = 10 µm.

771

Figure 9

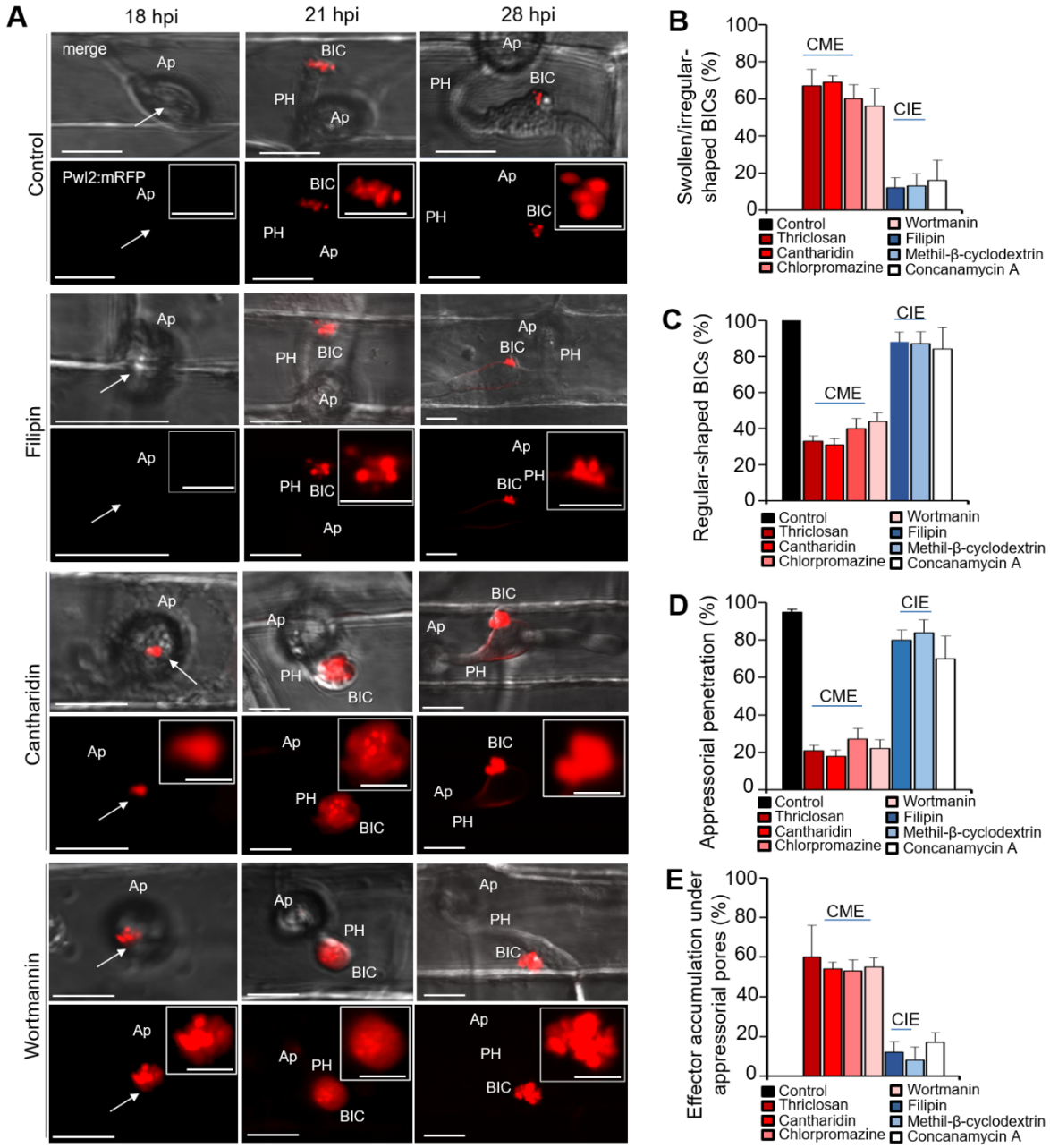


**Figure 9. Chemical inhibition of rice CME, but not of CIE, has a major impact on cytoplasmic effector localization and appressorial penetration. A.** Effects of chemical inhibition of Clathrin-mediated endocytosis (CME) and Clathrin-independent endocytosis (CIE) in the rice leaf sheath assay with strain KV209 expressing Pwl2:mRFP at 18, 21 and 28 hpi. Whereas inhibition of CIE showed minor effects on BIC functionality and effector uptake, the chemical inhibition of CME resulted in a significant accumulation of effector fluorescence under appressoria (Ap, white arrows at 18 hpi) as well as swollen BICs on primary hyphae (PH, 21 hpi) and bulbous IH (28hpi). Images in A (merged bright field and mRFP fluorescence) are projections of confocal optical sections. Insets show close-up views of the effector fluorescence. Bars = 10

783 µm and bars in the insert boxes = 5 µm. **B-E.** Quantification of swollen, irregular-shaped BICs
784 (B), regular-shaped BICs (C), appressorial penetration (D), and effector accumulation under
785 appressoria (E), in rice undergoing chemical treatment and infection by strain KV209 expressing
786 Pwl2:mRFP at 28 hpi. Bars are standard deviations. Three times 100 infection sites observed per
787 treatment.

788 Figure 10

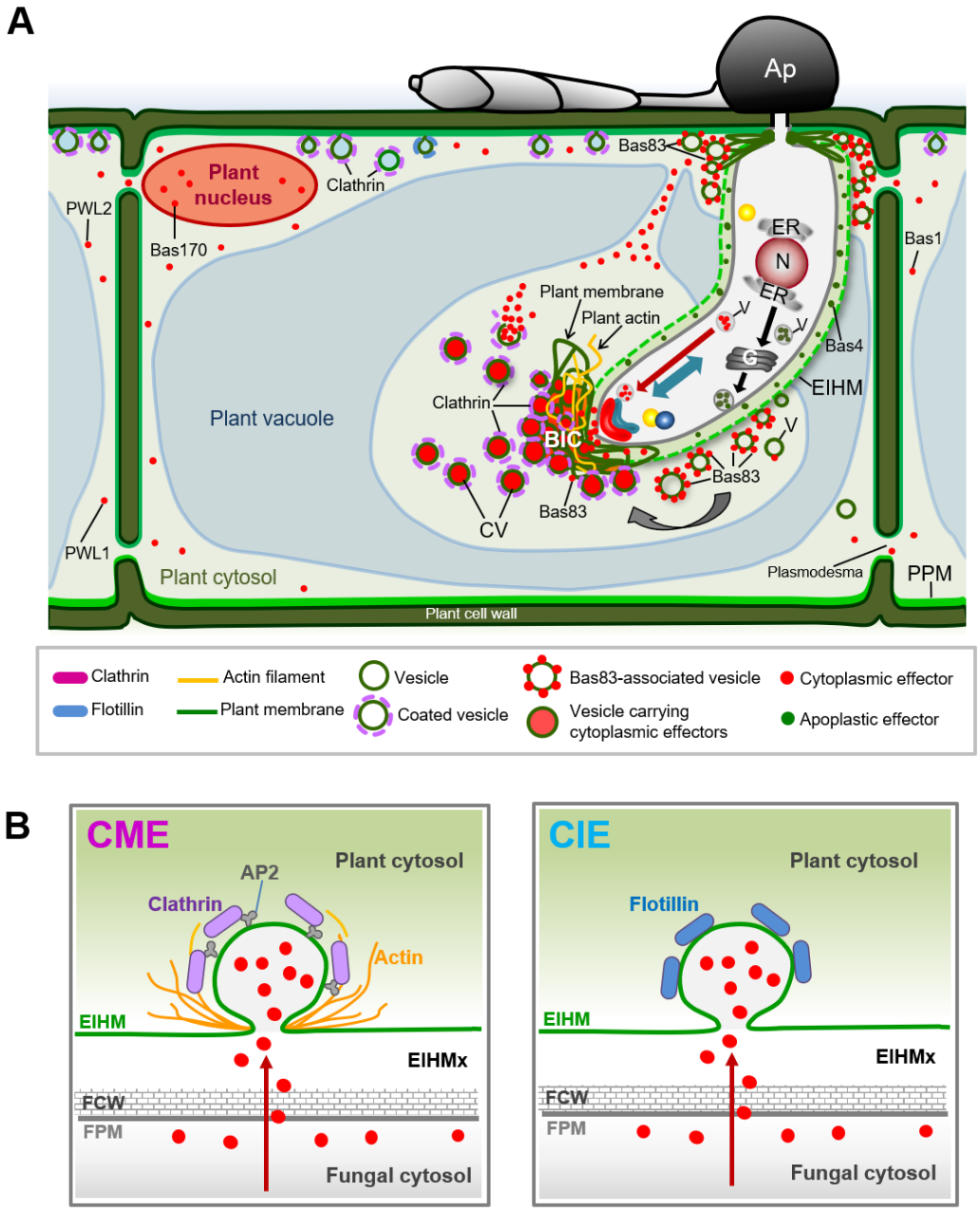


789
790 **Figure 10. Model for host effector translocation in rice-*M. oryzae* interactions. A.** This cartoon
791 represents a tip-BICs associated with primary hyphae (PH) growing at 22–24 h.p.i. (hours post-
792 inoculation) inside a rice cell, but similar mechanisms apply to side-BICs left behind after
793 differentiation of the first bulbous invasive hyphae (IH). At successful infection sites, apoplastic
794 effectors (dark green circles), including Biotrophy-associated secreted protein-4 (Bas4), are
795 secreted from the PH by conventional golgi-dependent secretion, which is blocked by treatment
796 with Brefeldin A (black arrows). Apoplastic effectors accumulate in the separate apoplastic
797 compartment enclosed by the EIHM (inside the dark green dashed line around the PH). In contrast,
798 cytoplasmic effectors (red circles), including known BIC markers Pwl2:FP, Pwl1:FP and Bas1:FP,

are secreted into BICs by a nonconventional, Brefeldin A-insensitive secretion system involving the exocyst and SNARE protein Sso1 (red arrows). Cytoplasmic effectors also accumulate inside the EIHM compartment around the BIC-associated cells, the PH and first differentiated bulbous IH cell (not shown), but not in the EIHM surrounding nonBIC-associated bulbous IH cells, which are tightly surrounded by the host vacuole. Our current study expands this model by showing that cytoplasmic effectors are packaged in dynamic vesicles inside BICs and in the host cytoplasm surrounding BICs, and that these effector vesicles co-localize with fluorescent plant plasma membrane markers LTi6B:GFP and FM 4-64, as well as clathrin-mediated endocytosis (CME) marker CLC1:eGFP. These co-localization studies, additional localization with plant actin in BICs, and functional analyses via VIGS and pharmacological inhibitors support CME as a major mechanism for effector translocation. We also report two novel cytoplasmic effectors, Bas83, which labels empty membrane vesicles possibly recruiting more host membrane to the BIC and the EIHM surrounding BIC-associated cells, and Bas170, which is delivered in vesicles to rice cytoplasm from under the appressorium and accumulates in the host nucleus even before growth of the primary hyphae. Cytoplasmic connections between cytoplasm surrounding BICs and cytoplasm on the host cell periphery would facilitate movement of translocated effectors to the host nucleus and other sites of action in the host cell, as well as movement of cytoplasmic effectors through plasmodesmata into surrounding host cells to prepare them for invasion. Key: N, fungal nucleus; ER, endoplasmic reticulum; G, Golgi apparatus; V, transport vesicle. **B.** Working models for vesicle formation and effector translocation in the rice-*M. oryzae* interaction through CME or clathrin-independent endocytosis (CIE). Although our current work supports a role for CME, some involvement of CIE in effector translocation cannot be totally ruled out. AP2, Adaptor Protein-2 complex; EIHM, extrainvasive hyphal membrane; EIHMx, extrainvasive hyphal matrix; FPM, fungal plasma membrane; FCW, fungal cell wall.

823 **REFERENCES**

824 Atkinson, H.A., Daniels, A., and Read, N.D. 2002. Live-cell imaging of endocytosis during
825 conidial germination in the rice blast fungus, *Magnaporthe grisea*. Fungal Gen. Biol.
826 37:233-244.

827 Beck, M., Heard, W., Mbengue, M., and Robatzek, S. 2012. The INs and OUTs of pattern
828 recognition receptors at the cell surface. Curr. Opin. Plant Biol. 15:367-374.

829 Bolte, S., Talbot, C., Boutte, Y., Catrice, O., Read, N.D., and Satiat-Jeunemaitre, B. 2004. FM-
830 dyes as experimental probes for dissecting vesicle trafficking in living plant cells. Journal
831 of Microscopy 214:159-173.

832 Bozkurt, T.O., Belhaj, K., Dagdas, Y.F., Chaparro-Garcia, A., Wu, C.-H., Cano, L.M., and
833 Kamoun, S. 2015. Rerouting of plant late endocytic trafficking toward a pathogen
834 interface. Traffic 16:204-226.

835 Bright, N.A., Lindsay, M.R., Stewart, A., and Luzio, J.P. 2001. The relationship between lumenal
836 and limiting membranes in swollen late endocytic compartments formed after wortmannin
837 treatment or sucrose accumulation. Traffic 2:631-642.

838 Carroll, A., Sweigard, J. A., and Valent, B. 1994. Improved vectors for selecting resistance to
839 hygromycin. 41:Article 5. https://newprairiepress.org/fgr/vol41/iss41/45/.

840 Catlett, N. L., Lee, B.-N., Yoder, O. C., and Turgeon, B. G. 2003. Split-marker recombination for
841 efficient targeted deletion of fungal genes. Fungal Genetics Newsletter 50:Article 4.
842 https://doi.org/10.4148/1941-4765.1150.

843 Chaparro-Garcia, A., Schwizer, S., Sklenar, J., Yoshida, K., Petre, B., Bos, J.I.B., Schornack, S.,
844 Jones, A.M.E., Bozkurt, T.O., and Kamoun, S. 2015. *Phytophthora infestans* RXLR-WY
845 effector AVR3a associates with dynamin-related protein 2 required for endocytosis of the
846 plant pattern recognition receptor FLS2. PLoS ONE 10:e0137071.

847 Chen, X., Irani, N.G., and Friml, J. 2011. Clathrin-mediated endocytosis: the gateway into plant
848 cells. Curr. Opin. Plant Biol. 14:674-682.

849 Collemare, J., Pianfetti, M., Houlle, A.E., Morin, D., Camborde, L., Gagey, M.J., Barbisan, C.,
850 Fudal, I., Lebrun, M.H., and Böhnert, H.U. 2008. *Magnaporthe grisea* avirulence gene
851 *ACE1* belongs to an infection-specific gene cluster involved in secondary metabolism. New
852 Phytol. 179:196-208.

853 Dagdas, Y.F., Pandey, P., Tumtas, Y., Sanguankiattichai, N., Belhaj, K., Duggan, C., Leary, A.Y.,
854 Segretin, M.E., Contreras, M.P., Savage, Z., Khandare, V.S., Kamoun, S., and Bozkurt,
855 T.O. 2018. Host autophagy machinery is diverted to the pathogen interface to mediate focal
856 defense responses against the Irish potato famine pathogen. eLife 7:e37476.
857 Dejonghe, W., and Russinova, E. 2017. Plant chemical genetics: From phenotype-based screens
858 to synthetic biology. Plant Physiology 174:5-20.
859 Dejonghe, W., Kuenen, S., Mylle, E., Vasileva, M., Keech, O., Viotti, C., Swerts, J., Fendrych,
860 M., Ortiz-Morea, F.A., Mishev, K., Delang, S., Scholl, S., Zarza, X., Heilmann, M.,
861 Kourelis, J., Kasprowicz, J., Nguyen, L.S.L., Drozdzecki, A., Van Houtte, I., Szatmári, A.-
862 M., Majda, M., Baisa, G., Bednarek, S.Y., Robert, S., Audenaert, D., Testerink, C.,
863 Munnik, T., Van Damme, D., Heilmann, I., Schumacher, K., Winne, J., Friml, J.,
864 Verstreken, P., and Russinova, E. 2016. Mitochondrial uncouplers inhibit clathrin-
865 mediated endocytosis largely through cytoplasmic acidification. Nat. Comm. 7:11710.
866 Di Rubbo, S., Irani, N. G., Kim, S. Y., Xu, Z.-Y., Gadeyne, A., Dejonghe, W., Vanhoutte, I.,
867 Persiau, G., Eeckhout, D., Simon, S., Song, K., Kleine-Vehn, J., Friml, J., De Jaeger, G.,
868 Van Damme, D., Hwang, I., and Russinova, E. 2013. The Clathrin Adaptor Complex AP-
869 2 mediates endocytosis of BRASSINOSTEROID INSENSITIVE1 in *Arabidopsis*. Plant
870 Cell 25:2986-2997.
871 Ding, X.S., Rao, C.S., and Nelson, R.S. 2007. Analysis of gene function in rice through virus-
872 induced gene silencing. Methods in molecular biology (Clifton, N.J.) 354:145-160.
873 Ding, X.S., Schneider, W.L., Chaluvadi, S.R., Mian, M.A.R., and Nelson, R.S. 2006.
874 Characterization of a Brome mosaic virus strain and its use as a vector for gene silencing
875 in monocotyledonous hosts. Mol. Plant-Microbe Interact. 19:1229-1239.
876 Dodds, P.N., and Rathjen, J.P. 2010. Plant immunity: towards an integrated view of plant-pathogen
877 interactions. Nat. Rev. Genet. 11:539-548.
878 Elsworth, B., Matthews, K., Nie, C.Q., Kalanon, M., Charnaud, S.C., Sanders, P.R., Chisholm,
879 S.A., Counihan, N.A., Shaw, P.J., Pino, P., Chan, J.A., Azevedo, M.F., Rogerson, S.J.,
880 Beeson, J.G., Crabb, B.S., Gilson, P.R., and de Koning-Ward, T.F. 2014. PTEX is an
881 essential nexus for protein export in malaria parasites. Nature 511:587-+.
882 Ewers, H., and Helenius, A. 2011. Lipid-mediated endocytosis. Cold Spring Harbor Perspectives
883 in Biology 3:10.1101/cshperspect.a004721.

884 Fan, L., Li, R., Pan, J., Ding, Z., and Lin, J. 2015. Endocytosis and its regulation in plants. Trends
885 in Plant Science 20:388-397.
886 Fawke, S., Doumane, M., and Schornack, S. 2015. Oomycete interactions with plants: infection
887 strategies and resistance principles. Microbiology and Molecular Biology Reviews 79:263-
888 280.
889 Fudal, I., Collemare, J., Böhnert, H.U., Melayah, D., and Lebrun, M.-H. 2007. Expression of
890 *Magnaporthe grisea* avirulence gene *ACE1* is connected to the initiation of appressorium-
891 mediated penetration. Eukaryotic Cell 6:546-554.
892 Giraldo, M.C., and Valent, B. 2013. Filamentous plant pathogen effectors in action. Nat. Rev.
893 Microbiol. 11:800-814.
894 Giraldo, M.C., Dagdas, Y.F., Gupta, Y.K., Mentlak, T.A., Yi, M., Martinez-Rocha, A.L., Saitoh,
895 H., Terauchi, R., Talbot, N.J., and Valent, B. 2013. Two distinct secretion systems facilitate
896 tissue invasion by the rice blast fungus *Magnaporthe oryzae*. Nat. Comm. 4:1996.
897 Gladieux, P., Condon, B., Ravel, S., Soanes, D., Maciel, J.L.N., Nhani, A., Chen, L., Terauchi, R.,
898 Lebrun, M.-H., Tharreau, D., Mitchell, T., Pedley, K.F., Valent, B., Talbot, N.J., Farman,
899 M., and Fournier, E. 2018. Gene flow between divergent cereal- and grass-specific lineages
900 of the rice blast fungus *Magnaporthe oryzae*. mBio 9:e01219-01217.
901 Grassart, A., Cheng, A.T., Hong, S.H., Zhang, F., Zenzer, N., Feng, Y., Briner, D.M., Davis, G.D.,
902 Malkov, D., and Drubin, D.G. 2014. Actin and dynamin2 dynamics and interplay during
903 clathrin-mediated endocytosis. Journal of Cell Biology 205:721-735.
904 Harder, D.E., and Mendgen, K. 1982. Filipin-sterol complexes in bean rust- and oat crown rust-
905 fungal/plant interactions: Freeze-etch electron microscopy. Protoplasma 112:46-54.
906 Hellens, R., Mullineaux, P., and Klee, H. 2000. Technical Focus: a guide to *Agrobacterium* binary
907 Ti vectors. Trends Plant Sci. 5:446-451.
908 Hicks, G.R., and Raikhel, N.V. 2010. Advances in dissecting endomembrane trafficking with
909 small molecules. Curr. Opin. Plant Biol. 13:706-713.
910 Himmelbach, A., Zierold, U., Hensel, G., Riechen, J., Douchkov, D., Schweizer, P., and Kumlehn,
911 J. 2007. A set of modular binary vectors for transformation of cereals. Plant Physiology
912 145:1192-1200.

913 Holsters, M., de Waele, D., Depicker, A., Messens, E., van Montagu, M., and Schell, J. 1978.
914 Transfection and transformation of *Agrobacterium tumefaciens*. Molecular and General
915 Genetics 163:181-187.
916 Howard, R.J., and Valent, B. 1996. Breaking and Entering: Host penetration by the fungal rice
917 blast pathogen *Magnaporthe grisea*. Annu. Rev. Microbiol. 50:491-512.
918 Johnson, A., Gnyliukh, N., Kaufmann, W.A., Narasimhan, M., Vert, G., Bednarek, S.Y., and
919 Friml, J. 2020. Experimental toolbox for quantitative evaluation of clathrin-mediated
920 endocytosis in the plant model *Arabidopsis*. Journal of Cell Science 133:jcs248062.
921 Jones, K., Zhu, J., Jenkinson, C.B., Kim, D.W., Pfeifer, M.A., and Khang, C.H. 2021. Disruption
922 of the interfacial membrane leads to *Magnaporthe oryzae* effector re-location and lifestyle
923 switch during rice blast disease. Frontiers in Cell and Developmental Biology
924 9:10.3389/fcell.2021.681734.
925 Kaksonen, M., and Roux, A. 2018. Mechanisms of clathrin-mediated endocytosis. Nat. Rev. Mol.
926 Cell Biol. 19:313-326.
927 Kale, S.D., Gu, B., Capelluto, D.G.S., Dou, D., Feldman, E., Rumore, A., Arredondo, F.D.,
928 Hanlon, R., Fudal, I., Rouxel, T., Lawrence, C.B., Shan, W., and Tyler, B.M. 2010.
929 External lipid PI3P mediates entry of eukaryotic pathogen effectors into plant and animal
930 host cells. Cell 142:284-295.
931 Kankanala, P., Czymmek, K., and Valent, B. 2007. Roles for rice membrane dynamics and
932 plasmodesmata during biotrophic invasion by the blast fungus. Plant Cell 19:706-724.
933 Kato, H. 1974. Epidemiology of rice blast disease. Review of Plant Protection Research 7:1-20.
934 Kershaw, M. J., and Talbot, N. J. 2009. Genome-wide functional analysis reveals that infection-
935 associated fungal autophagy is necessary for rice blast disease. Proceedings of the National
936 Academy of Sciences U.S.A. 106:15967-15972.
937 Khang, C.H., Park, S., Rho, H., Lee, Y., and Kang, S. 2006. *Agrobacterium tumefaciens*-mediated
938 transformation and mutagenesis of filamentous fungi *Magnaporthe grisea* and *Fusarium*
939 *oxysporum*. in: Agrobacterium Protocols, K. Wang, ed. Humana Press, Totowa.
940 Khang, C.H., Berruyer, R., Giraldo, M.C., Kankanala, P., Park, S.-Y., Czymmek, K., Kang, S.,
941 and Valent, B. 2010. Translocation of *Magnaporthe oryzae* effectors into rice cells and
942 their subsequent cell-to-cell movement. Plant Cell 22:1388-1403.

943 Kleemann, J., Rincon-Rivera, L.J., Takahara, H., Neumann, U., Ver Loren van Themaat, E., van
944 der Does, H.C., Hacquard, S., Stüber, K., Will, I., Schmalenbach, W., Schmelzer, E., and
945 O'Connell, R.J. 2012. Sequential delivery of host-induced virulence effectors by
946 appressoria and intracellular hyphae of the phytopathogen *Colletotrichum higginsianum*.
947 PLoS Path. 8:e1002643.
948 Konopka, C.A., Backues, S.K., and Bednarek, S.Y. 2008. Dynamics of Arabidopsis Dynamin-
949 Related Protein 1C and a Clathrin Light Chain at the Plasma Membrane Plant Cell
950 20:1363-1380.
951 Larson, E. R., Van Zelm, E., Roux, C., Marion-Poll, A., and Blatt, M. R. 2017. Clathrin heavy
952 chain subunits coordinate endo- and exocytic traffic and affect stomatal movement. Plant
953 Physiol. 175:708-720.
954 Leung, H., Borromeo, E.S., Bernardo, M.A., and Notteghem, J.L. 1988. Genetic analysis of
955 virulence in the rice blast fungus *Magnaporthe grisea*. Phytopathology 78:1227-1233.
956 Li, R., Liu, P., Wan, Y., Chen, T., Wang, Q., Mettbach, U., Baluška, F., Samaj, J., Fang, X., Lucas,
957 W.J., and Lin, J. 2012. A membrane microdomain-associated protein, *Arabidopsis* Flot1,
958 is involved in a clathrin-independent endocytic pathway and is required for seedling
959 development. Plant Cell 24 2105-2122
960 Lo Presti, L., and Kahmann, R. 2017. How filamentous plant pathogen effectors are translocated
961 to host cells. Curr. Opin. Plant Biol. 38:19-24.
962 Lo Presti, L., Zechmann, B., Kumlehn, J., Liang, L., Lanver, D., Tanaka, S., Bock, R., and
963 Kahmann, R. 2017. An assay for entry of secreted fungal effectors into plant cells. New
964 Phytol. 213:956-964.
965 Lo Presti, L., Lanver, D., Schweizer, G., Tanaka, S., Liang, L., Tollot, M., Zuccaro, A., Reissmann,
966 S., and Kahmann, R. 2015. Fungal effectors and plant susceptibility. Annual Review of
967 Plant Biology 66:513-545.
968 Ludwig, N., Reissmann, S., Schipper, K., Gonzalez, C., Assmann, D., Glatter, T., Moretti, M., Ma,
969 L.-S., Rexer, K.-H., Snetselaar, K., and Kahmann, R. 2021. A cell surface-exposed protein
970 complex with an essential virulence function in *Ustilago maydis*. Nature Microbiology
971 6:722-730.
972 Manning, V.A., and Ciuffetti, L.M. 2005. Localization of Ptr ToxA produced by *Pyrenophora*
973 *tritici-repentis* reveals protein import into wheat mesophyll cells. Plant Cell 17:3203-3212.

974 Maranda, B., Brown, D., Bourgoin, S., Casanova, J.E., Vinay, P., Ausiello, D.A., and Marshansky,
975 V. 2001. Intra-endosomal pH-sensitive recruitment of the Arf-nucleotide exchange factor
976 ARNO and Arf6 from cytoplasm to proximal tubule endosomes. Journal of Biological
977 Chemistry 276:18540-18550.
978 Mbengue, M., Bourdais, G., Gervasi, F., Beck, M., Zhou, J., Spallek, T., Bartels, S., Boller, T.,
979 Ueda, T., Kuhn, H., and Robatzek, S. 2016. Clathrin-dependent endocytosis is required for
980 immunity mediated by pattern recognition receptor kinases. Proceedings of the National
981 Academy of Sciences 113:11034-11039.
982 Mentlak, T.A., Kombrink, A., Shinya, T., Ryder, L.S., Otomo, I., Saitoh, H., Terauchi, R.,
983 Nishizawa, Y., Shibuya, N., Thomma, B.P., and Talbot, N.J. 2012. Effector-mediated
984 suppression of chitin-triggered immunity by *Magnaporthe oryzae* is necessary for rice blast
985 disease. Plant Cell 24:322-335.
986 Mochizuki, S., Minami, E., and Nishizawa, Y. 2015. Live-cell imaging of rice cytological changes
987 reveals the importance of host vacuole maintenance for biotrophic invasion by blast
988 fungus, *Magnaporthe oryzae*. MicrobiologyOpen 4:952-966.
989 Mosquera, G., Giraldo, M.C., Khang, C.H., Coughlan, S., and Valent, B. 2009. Interaction
990 transcriptome analysis identifies *Magnaporthe oryzae* BAS1-4 as biotrophy-associated
991 secreted proteins in rice blast disease. Plant Cell 21:1273-1290.
992 Narasimhan, M., Johnson, A., Prizak, R., Kaufmann, W.A., Tan, S., Casillas-Pérez, B., and Friml,
993 J. 2020. Evolutionarily unique mechanistic framework of clathrin-mediated endocytosis in
994 plants. eLife 9:e52067.
995 Nishimura, T., Mochizuki, S., Ishii-Minami, N., Fujisawa, Y., Kawahara, Y., Yoshida, Y., Okada,
996 K., Ando, S., Matsumura, H., Terauchi, R., Minami, E., and Nishizawa, Y. 2016.
997 *Magnaporthe oryzae* glycine-rich secretion protein, Rbf1 critically participates in
998 pathogenicity through the focal formation of the biotrophic interfacial complex. PLoS Path.
999 12:e1005921.
1000 Nishizawa, Y., Mochizuki, S., Yokotani, N., Nishimura, T., and Minami, E. 2016. Molecular and
1001 cellular analysis of the biotrophic interaction between rice and *Magnaporthe oryzae* –
1002 Exploring situations in which the blast fungus controls the infection. Physiol. Mol. Plant
1003 Pathol. 95:70-76.

1004 O'Connell, R.J., and Panstruga, R. 2006. Tête à tête inside a plant cell: establishing compatibility
1005 between plants and biotrophic fungi and oomycetes. New Phytol. 171:699-718.
1006 Otto, G.P., and Nichols, B.J. 2011. The roles of flotillin microdomains – endocytosis and beyond.
1007 Journal of Cell Science 124:3933-3940.
1008 Park, S.H., Park, J., and Smith, R.H. 2001. Herbicide and insect resistant elite transgenic rice.
1009 Journal of Plant Physiology 158:1221-1226.
1010 Petre, B., and Kamoun, S. 2014. How do filamentous pathogens deliver effector proteins into plant
1011 cells? PLoS. Biol. 12:e1001801.
1012 Petre, B., Contreras, M.P., Bozkurt, T.O., Schattat, M.H., Sklenar, J., Schornack, S., Abd-El-
1013 Haliem, A., Castells-Graells, R., Lozano-Durán, R., Dagdas, Y.F., Menke, F.L.H., Jones,
1014 A.M.E., Vossen, J.H., Robatzek, S., Kamoun, S., and Win, J. 2021. Host-interactor screens
1015 of *Phytophthora infestans* RXLR proteins reveal vesicle trafficking as a major effector-
1016 targeted process. Plant Cell 33:1447-1471.
1017 Postma, J., Liebrand, T.W.H., Bi, G., Evrard, A., Bye, R.R., Mbengue, M., Kuhn, H., Joosten,
1018 M.H.A.J., and Robatzek, S. 2016. Avr4 promotes Cf-4 receptor-like protein association
1019 with the BAK1/SERK3 receptor-like kinase to initiate receptor endocytosis and plant
1020 immunity. New Phytol. 210:627-642.
1021 Qi, X., Pleskot, R., Irani, N.G., and Van Damme, D. 2018. Meeting report – Cellular gateways:
1022 expanding the role of endocytosis in plant development. Journal of Cell Science
1023 131:jcs222604.
1024 Reynolds, G.D., Wang, C., Pan, J., and Bednarek, S.Y. 2018. Inroads into internalization: Five
1025 years of endocytic exploration. Plant Physiology 176:208-218.
1026 Robinson, D.G., Jiang, L.W., and Schumacher, K. 2008. The endosomal system of plants: Charting
1027 new and familiar territories. Plant Physiology 147:1482-1492.
1028 Rodal, S.K., Skretting, G., Garred, O., Vilhardt, F., van Deurs, B., and Sandvig, K. 1999.
1029 Extraction of cholesterol with methyl-beta-cyclodextrin perturbs formation of clathrin-
1030 coated endocytic vesicles. Molecular Biology of the Cell 10:961-974.
1031 Sachse, M., Urbe, S., Oorschot, V., Strous, G.J., and Klumperman, J. 2002. Bilayered clathrin
1032 coats on endosomal vacuoles are involved in protein sorting toward lysosomes Molecular
1033 Biology of the Cell 13:1313-1328

1034 Sakulkoo, W., Oses-Ruiz, M., Garcia, E.O., Soanes, D.M., Littlejohn, G.R., Hacker, C., Correia,
1035 A., Valent, B., and Talbot, N.J. 2018. A single fungal MAP kinase controls plant cell-to-
1036 cell invasion by the rice blast fungus. Science 359:1399-1403.
1037 Serrano, M., Robatzek, S., Torres, M., Kombrink, E., Somssich, I.E., Robinson, M., and Schulze-
1038 Lefert, P. 2007. Chemical interference of pathogen-associated molecular pattern-triggered
1039 immune responses in Arabidopsis reveals a potential role for fatty-acid synthase type II
1040 complexderived lipid signals. Journal of Biological Chemistry 282:6803-6811.
1041 Spallek, T., Beck, M., Ben Khaled, S., Salomon, S., Bourdais, G., Schellmann, S., and Robatzek,
1042 S. 2013. ESCRT-I mediates FLS2 endosomal sorting and plant immunity. PLoS Genetics
1043 9:e1004035.
1044 Stark-Urnau, M., and Mendgen, K. 1995. Sequential deposition of plant glycoproteins and
1045 polysaccharides at the host-parasite interface of *Uromyces vignae* and *Vigna sinensis*:
1046 Evidence for endocytosis and secretion. Protoplasma 186:1-11.
1047 Sweigard, J. A., Carroll, A. M., Kang, S., Farrall, L., Chumley, F. G., and Valent, B. 1995.
1048 Identification, cloning, and characterization of *PWL2*, a gene for host species specificity in
1049 the rice blast fungus. Plant Cell 7:1221-1233.
1050 Trusch, F., Loebach, L., Wawra, S., Durward, E., Wuensch, A., Iberahim, N.A., de Bruijn, I.,
1051 MacKenzie, K., Willems, A., Toloczko, A., Diéguez-Uribeondo, J., Rasmussen, T.,
1052 Schrader, T., Bayer, P., Secombes, C.J., and van West, P. 2018. Cell entry of a host-
1053 targeting protein of oomycetes requires gp96. Nat. Comm. 9:2347.
1054 Valent, B., and Chumley, F.G. 1991. Molecular genetic analysis of the rice blast fungus,
1055 *Magnaporthe grisea*. Annu. Rev. Phytopathol. 29:443-467.
1056 Valent, B., Singh, P.K., He, X., Farman, M., Tosa, Y., and Braun, H.J. 2020. Blast diseases:
1057 Evolution and challenges of a staple food crop fungal pathogen. Pages 267-292 in:
1058 Emerging Plant Diseases and Global Food Security, J.B. Ristaino and A. Records, eds.
1059 American Phytopathological Society Press, St. Paul, MN.
1060 Van den Ackerveken, G. 2017. Seeing is believing: imaging the delivery of pathogen effectors
1061 during plant infection. New Phytol. 216:8-10.
1062 Wang, L.H., Rothberg, K.G., and Anderson, R.G. 1993. Misassembly of clathrin lattices on
1063 endosomes reveals a regulatory switch for coated pit formation Journal of Cell Biology
1064 123:1107-1117.

1065 Wang, S., Boevink, P.C., Welsh, L., Zhang, R., Whisson, S.C., and Birch, P.R.J. 2017. Delivery
1066 of cytoplasmic and apoplastic effectors from *Phytophthora infestans* haustoria by distinct
1067 secretion pathways. New Phytol. 216:205-215.
1068 Wawra, S., Trusch, F., Matena, A., Apostolakis, K., Linne, U., Zhukov, I., Stanek, J., Koźmiński,
1069 W., Davidson, I., Secombes, C.J., Bayer, P., and van West, P. 2017. The RxLR motif of
1070 the host targeting effector AVR3a of *Phytophthora infestans* is cleaved before secretion.
1071 Plant Cell 29:1184-1195.
1072 Xu, J.-R., Staiger, C.J., and Hamer, J.E. 1998. Inactivation of the mitogen-activated protein kinase
1073 Mps1 from the rice blast fungus prevents penetration of host cells but allows activation of
1074 plant defense responses. Proceedings of the National Academy of Sciences U.S.A.
1075 95:12713-12718.